STUDY OF INTERDIFFUSION AND GROWTH OF INTERMETALLIC COMPOUNDS IN BIMETALLIC LAYERS OF ALPHA BRASS AND Al-Mg ALLOY

by

RATAN KOTA

THESIS

Presented to the Faculty of the Graduate School of

The University of Texas at Arlington in Partial Fulfillment

of the Requirements for the Degree of

Master of Science in Materials Science & Engineering at

The University of Texas at Arlington

August 2020

Supervising Committee:

Choong-Un Kim, Supervising Professor

Seong Jin Koh

Nancy Michael

ACKNOWLEDGEMENTS

I would like to thank my advisor Prof. Choong-Un Kim for providing his guidance and support throughout my research. I am thankful to him for his help and encouragement. I would also like to thank my committee members Dr Koh and Dr Michael for their valuable feedback. I would also like to thank all the faculty members of the MSE department.

I would also like to thank all my current group members Geng Ni, Alison Osmanson, Hossein Madanipour, Yiram Kim, Mohsen Tajedhani, Sara Rosa, Yvonne Albert, Manasi Puranik who helped me during my research and motivated me in right direction.

I would like to thank Dr. Jiang and his staff at Characterization Centre for Materials and Biology, for training me on various equipment.

I would also like to thank my parents, my brother Sandeep and my cousin Rahul for encouraging and supporting me throughout my career. I want to dedicate my thesis to them.

August 2020

ABSTRACT

STUDY OF INTERDIFFUSION AND GROWTH OF INTERMETALLIC COMPOUNDS IN BIMETALLIC LAYERS OF ALPHA BRASS AND Al-Mg ALLOY

Ratan Kota, M.S.

The University of Texas at Arlington, 2020

Supervising Professor: Choong-Un Kim

This work aims to study the formation of Inter Metallic Compounds (IMC's) and their growth rate in Brass and Al-Mg alloy. This diffusion couple consists of four elements Aluminum, Copper, Zinc and Magnesium. Aluminum and Copper are major diffusing elements. Brass-Aluminum bimetal is an advanced structural material and used as a cladding material. This bimetal is produced by cold roll bonding and is mechanically bonded. To increase the adhesive strength of these bimetal layers, the sample is subjected to heat treatment which leads to the formation of Inter Metallic Compounds (IMC). Heat treatments are generally done above the recrystallization temperature of the elements. The recrystallization temperature of the all the four elements with highest melting point is Copper (1085°C) which is about 270°C and the lowest melting point of the four elements is Zinc which is

about 420°C. Hence the temperatures in between are good for heat treatment. In this research, temperatures 350°C and 400°C are chosen for heat treatment of samples.

In first part of this research the samples are cut from a cold rolled bonded three-layer brass-aluminum bimetal. These samples are heat treated in a tube furnace at chosen temperatures of 350°C and 400°C for different lengths of times. SEM analysis of the finely polished sample surfaces showed five distinct layers of IMC in between brass and aluminum layers.

In the second part of this work, EDS analysis and XRD analysis is done on samples to find the chemical composition of these identified five layers. It was also observed that the kirkendall voids that were present in the sample coalesced as the heat treatment time increased and formed as a crack. The formation of crack stopped diffusion of elements across IMC's, when samples were heat treated at 400°C for more than 20 hours. It was also observed that, of the five layers formed, the layer adjacent to α-brass is found to be duplex brass and is formed because of uphill diffusion of zinc and the $Mg_2Cu_6Al_5$ formed adjacent to $CuAl_2$ is because of uphill diffusion of Magnesium.

In the final part, trend analysis of IMC thickness is done. The obtained data is plotted as thickness vs square root of time. The resulting graphs show that the diffusion across IMC's follows parabolic law.

Table of Contents

List of Figures

List of Tables

List of Graphs

CHAPTER 1

INTRODUCTION AND BACKGROUND

1.1 Overview of Bimetals

A bimetal is a combination of two different metals. The difference between a bimetal and an alloy is that bimetal consists of layers of two different metals. Bimetals have wide range of applications in industries. Few of the applications are in corrosion resistance materials, wear resistant materials, tool materials, thermal bimetals etc. Some applications of bimetals include coating a steel can with tin to prevent it from rust and coating a U.S. penny with copper on a 95% Zinc coin to reduce costs. Multilayer metallic materials are being widely used in automobiles, ships, aircraft and many other manufacturing industries. It has been proven that they have superior strength, toughness, ductility, corrosion resistance and cost effectiveness when compared to single layer materials [1][2]. Depending on the requirement, bimetals can be produced as wire, sheet, strip etc. There are different methods to produce bimetals, but the important goal in production is to obtain a strong bond between layers. There can be three different combinations of materials state: liquid+ liquid or liquid+ solid or solid+ solid contact at the interface during a bimetal production. Cast surfacing, continuous casting, centrifugal casting, explosive welding, cold roll bonding etc. [3] are few methods of producing bimetals.

Cold Roll Bonding is used in the production of thin bimetals consisting of copper, aluminum, steel, titanium etc. The production of bimetals by cold roll bonding process consists of steps

such as preparation of the initial components surfaces, cold rolling. Preparation of sample surface is degreasing and roughening of surface to remove oxide layers and give good friction to surfaces for good adhesion when rolled. The adhesion of metal layers takes place because of mechanical bonding. This bonding is not a strong bond. Hence the bimetals are subjected to heat treatment to increase bond strength. When bimetals are subjected to heat treatment, inter diffusion of atoms takes place, because of which Inter Metallic Compounds are formed. Formation of IMC can change the mechanical bond to chemical bond, which is stronger. However, excessive heat treatment promoted the growth of IMC's and subsequently lead to the formation of cracks, leading to the delamination of bimetal sheet as observed in [4]. When there are multiple components in a system and there is a significant interaction between components, the multi component diffusion should be non-linear as mentioned in [5].

1.2 Roll Bonding

Rolling is one of the metal forming processes and is a bulk forming process, because of severe deformation and a massive shape change. For this process, the surfaces of desired metal plates to be rolled are roughened using metal brushes to remove any dirt or oxide layers. The plates are then passed through rotating rolls, which will compress and draw the plates to form a sheet consisting of layers of metals bonded. However, the volume of sheets after rolling will be same as volume of plates before rolling.

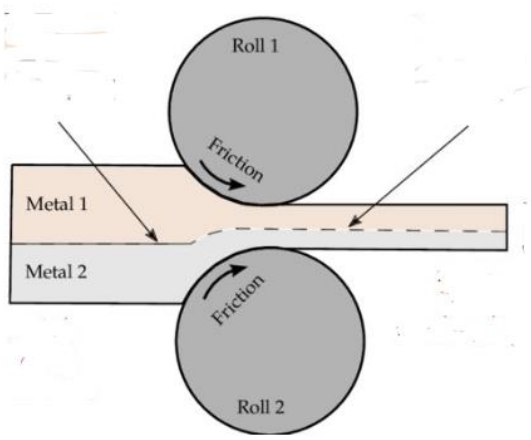

Fig 1: Schematic of roll bonding process [6]

Based on the temperature at which the process is carried out, the roll bonding process can be categorized into hot rolling and cold rolling. If the temperature at which the metal/ metals are rolled is above recrystallization temperature, it is called hot rolling. If the temperature is below recrystallization temperature, it is called cold rolling. There is lot of research going on diffusion and IMC formation in diffusion couples formed by roll bonding [7]–[12].

When the metal plate is subjected to reduction in size through rolling process, the grains are elongated in the direction of rolling. By heat treatment of sample, recrystallization of grains takes place. Therefore, the area of study on the sample will be the cross-sectional area in the direction of rolling.

1.3 Heat Treatment

It is a thermal process used to alter the physical/ chemical/ mechanical properties of the metal by heating it above its critical temperature and below its melting temperature. Based on the rate

of cooling, the bulk heat treatment can be categorized as Annealing, Annealing and Hardening. In general, the critical temperature is 0.4 T_m (melting temperature) of metal. It is during cooling, the phases tend to form or transform.

Fig 2: Flowchart showing the steps involved in a heat treatment process

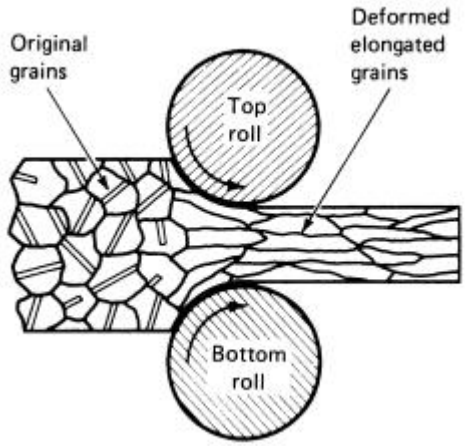

Fig 3: Schematic of change in grain size due to rolling[13]

1.3.1 Annealing:

Annealing is a heat treatment process in which a metal is heated beyond its critical temperature and soaked at that temperature for desired amount of time and then left to cool in the furnace. Rate of cooling is very slow in annealing. Annealing is done to relieve internal stresses and to refine the grain structure. It also increases ductility, toughness, machinability of a metal.

1.3.2 Normalizing:

Normalizing is a heat treatment process in which a metal is heated beyond its critical

temperature and cooled in air at room temperature. Rate of cooling is comparatively higher than annealing. Normalizing of metals form smaller grains/ crystals because of faster cooling. This leads to strengthening of metal. It reduces internal stresses caused because of work hardening.

1.3.3 HARDENING:

Hardening is a heat treatment process in which a metal is heated beyond its critical temperature and cooled in a water or oil bath. Rate of cooling is rapid in this case. Hardness of metal increases. However, normalizing and hardening does not have much impact on non-ferrous metals. But in this research, annealing is done at 350, 400°C for different amounts of times.

1.4 Diffusion

Diffusion is essentially migration or mass transfer of atoms. There are different types of diffusion based on state of matter (solid, liquid or gas). This research is mainly focusing on solid state diffusion. Solids as liquids and gases have molecules, ions or atoms. The atoms in a solid material are arranged in an ordered structure or pattern, these patterns are called crystal lattice or crystal structures. In a perfect crystal, there are no defects. However, a normal crystal has many defects such as point, line and planar which allow the atoms to move. This process of atomic movement can be called as diffusion. Diffusion can happen because of presence of vacancies (point defects) in crystals. Vacancy diffusion can be categorized as substitutional and interstitial diffusion.

Atoms tend to move from places of higher concentration to places of lower concentration. A relation for a mass flux (J) of atoms diffusing through a distance ∂x due to change in concentration ∂C is given by Fick's first law of diffusion.

$$J \propto \frac{\partial C}{\partial x}$$

$$J = -D\frac{\partial C}{\partial x}$$

Where,

J is mass flux of atoms

D is diffusion coefficient or diffusivity

$\frac{\partial C}{\partial x}$ is concentration gradient

During diffusion, if concentration does not change with time, then it is called as a steady state diffusion. When there is a concentration change with respect to both time and distance, it is called as non-steady state diffusion. In this case Fick's first law cannot be used. Non- steady state diffusion is characterized by Fick's second law, which is

$$\partial C/\partial t = D\ \partial^2 C/\partial x^2$$

Where,

$\partial C/\partial t$ is change in concentration with time

D is diffusivity

As mentioned earlier, diffusion is a mass transfer which happens because of change in concentration. For diffusion to happen, the atoms must move, for them to move, they need some form of energy. When an object is heated, the atoms in it absorb energy and will reach an unstable state. They tend to move to meta-stable or stable state by losing some energy (kinetic energy).

This energy is lost by movement of atoms which is otherwise called as diffusion. However, for diffusion to happen the system has to have enough energy (activation energy). When atoms are given activation energy (E_a), they tend to diffuse into lattice defects such as grain boundaries and dislocations and can lower their free energies.

Diffusion can be categorized into two types based on two types of solid solutions.

Interstitial Diffusion: If the solute atoms diffuse from one interstitial site to the other in a solid solution, it is called as interstitial diffusion.

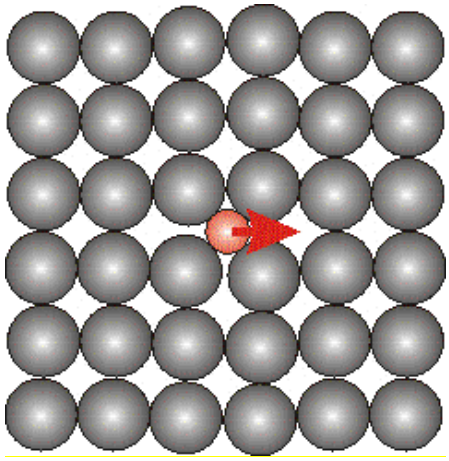

Fig4: Schematic of interstitial diffusion

Substitutional Diffusion: If the solute atoms diffuse or move in a substitutional solid solution, it is called substitutional diffusion.

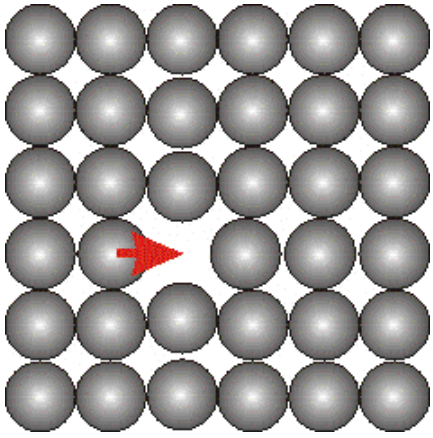

Fig5: Schematic of substitutional diffusion by vacancy mechanism

The mechanism of substitutional diffusion was earlier believed to be because of direct interchange or ring mechanism of atomic interchange. It can be better explained by vacancy mechanism.

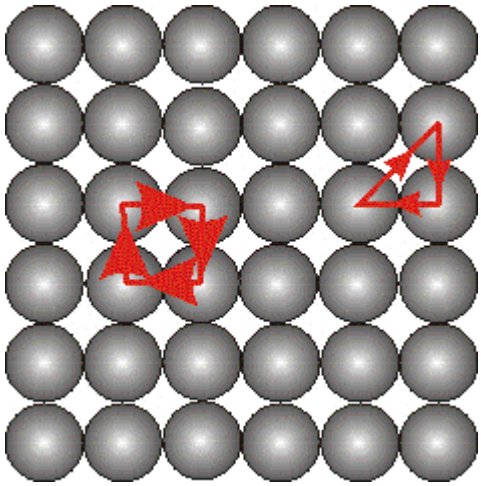

Fig6: Schematic showing interchange and ring mechanisms in substitutional diffusion

Interstitial diffusion is generally faster than substitutional diffusion. Because of presence of lot of vacancies around the solute atoms in a solvent, they tend to move faster. In a substitutional

solid solution case, both the solute and solvent are of same size. So, the solute atoms can only move through the limited vacancies.

1.5 Hume-Rothery rules

There are two types of solid solutions 1) Interstitial 2) Substitutional. Some solid solutions have solubility limit i.e. the amount of solute that can dissolve in a solvent has a limit. Carbon in steel and zinc in brass have solubility limit, while copper and nickel does not show any such solubility limit i.e., they have complete solid solubility. Hume-Rothery found some empirical rules that can be applicable to both interstitial and substitutional diffusion. The following are the rules for Interstitial and Substitutional solid solution cases.

Interstitial solute case

1. Solute atoms must be smaller than solvent atoms for them to fit into the interstitial spaces of the solvent crystal lattice.
2. Both solute and solvent must have similar electronegativity.

Substitutional solute case

1. Solvent and solute crystal structures must be identical (structure factor).
2. The difference between the solute and solvent radii (atomic size) should not be greater than 15% (size factor).
3. If the difference of the electronegativity between solute and solvent is higher, then there is a higher possibility of IMC formation instead of solid solution (electronegativity factor).
4. A metal with higher valence will dissolve in a metal with lower valence. The complete

solubility is possible only when both solute and solvent have the same valence (valence factor).

When these rules are not obeyed by the metals, there is chance for the formation of Inter Metallic Compound (IMC).

1.6 Inter Metallic Compound (IMC) formation

IMCs are highly ordered solid-state compounds. As mentioned earlier, the diffusion of elements does not take place in a random moment of vacancies as it would disturb the arrangement of atoms in their respective crystalline structure. When a diffusion couple is subjected to solution heat treatment, an intermetallic compound is formed in between because of diffusion. A hypothetical diffusion couple and formation of IMC and their concentration profile is discussed in [14]

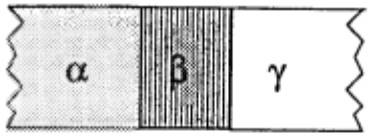

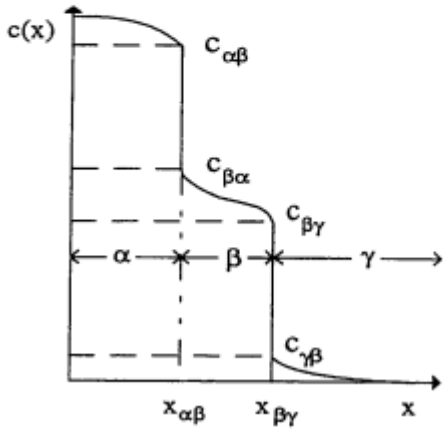

Fig 7: Schematic of diffusion in hypothetical diffusion couple α,γ giving an IMC β and their concentration profile[14]

When diffusion continues to take place after the formation of IMC as shown in fig 6, a new IMC formation can take place near the interface boundary. These new IMC's from as a thin layer and tend to grow. Diffusion allows the newly formed IMC's to grow normal to the interface. When the volume diffusion occurs, then the IMC layer growth follows parabolic law [7]. Significance of parabolic growth is also mentioned in [15]–[23].

$$x = k.t^{-(1/2)}$$

where,

x is thickness of IMC

k is constant

t is time

There are four types of diffusion path, an atom can diffuse. They are surface diffusion, lattice diffusion, grain boundary diffusion and diffusion along dislocation (pipe diffusion). Substitutional and interstitial diffusions are lattice diffusions.

The activation energies required for these diffusions are given by Q, Q_s, Q_d, Q_{gb} for lattice, surface, pipe, grain boundary diffusions respectively. It is easy for a surface atom to diffuse as it has less number of surrounding atoms, therefore the activation energy required will be less and it is difficult for an atom to diffuse through lattice. When the activation energies are

arranged in an ascending order.

$Q_s < Q_{gb} \leq Q_d < Q$

Let D, D_s, D_d, D_{gb} be the diffusivities of lattice, surface, pipe, grain boundary diffusions respectively. These diffusivities depend on the activation energies. The lesser the activation energy required to diffuse; the higher will be the diffusivity. Therefore, the relation of these diffusivities can be given as

$D < D_d \leq D_{gb} < D_s$

Grain boundary diffusion plays a major role in IMC growth rate. Inside a grain the atoms are ordered, while the disordered structure can be observed at grain boundaries. This disordered structure allows faster diffusion of atoms. Grain boundary diffusion slows down when impurities/alloying elements are present because the impurities accumulate at grain boundaries.

Fig 8: Schematic of diffusion of elements along grain boundary [24]

When atoms move along grain boundary, the grain size changes where movement along grain boundary causes densification[25]. Formation and growth of IMC's can cause fracture either because of brittle nature of IMC's or because of insufficient bond strength among the IMC interfaces as mentioned in [26].

The condition for a phase transformation to occur is reduction in free energy of elements which happens because of diffusion and formation of IMC's. The formation of IMC's and diffusion can be used to predict material properties and microstructure[27].

1.7 Cu-Al phase diagram

The Cu-Al binary system has been studied for a long time. Duralumin (Al(rich)- cu alloys) are mainly used in aerospace industries. Solubility of copper in aluminum is about 5%. Copper and its alloys are widely used in industries as electrical conductor, automobile radiators, pressure vessels, and so on. Cu rich aluminum alloys are called aluminum bronzes. The solubility of aluminum in copper is from 5-11%. They are also used in aerospace and naval industries because of their good strength and corrosion resistance. Cu-Al intermetallic compounds are also widely studied because of use of copper wire bond in microelectronics industry and electromigration taking place in microelectronic components.

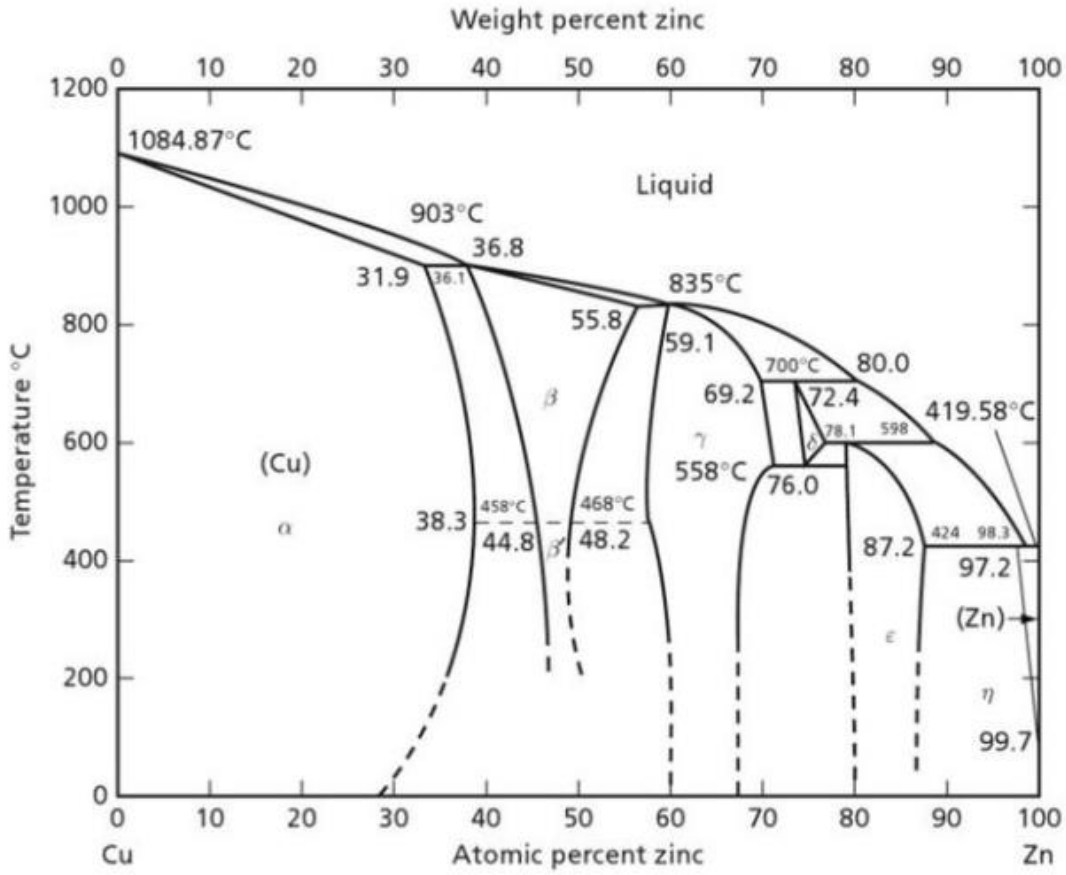

Fig 9: Phase diagram of Cu-Al showing atomic and weight percentage of Copper [28]

According to the phase diagram shown in Fig 9, six IMCs can be seen to exist at temperature 350°C. These phases are θ-Al_2Cu, η-CuAl, ξ-Cu_4Al_3, δ–Cu_3Al_2, γ-Cu_9Al_4, and α_2- Cu_3Al, from the Al-rich side. At 400°C all the five phases other than α_2- Cu_3Al can be seen.

1.8 Cu-Zn phase diagram

Cu-Zn alloys are brasses. Brasses are decorative alloys mainly used in ornaments because of their

bright surface. By adding different elements to brass, they can be used in different industries. When more copper is added to a brass, it can be called as riveting brass because of increased malleability. Addition of tin gives corrosion resistance to brass and therefore is used in naval industry. Addition of lead can increase the machinability of brass. Addition of manganese increases the strength and is called high tensile brass. Addition of arsenic makes it dezincification resistant brass.

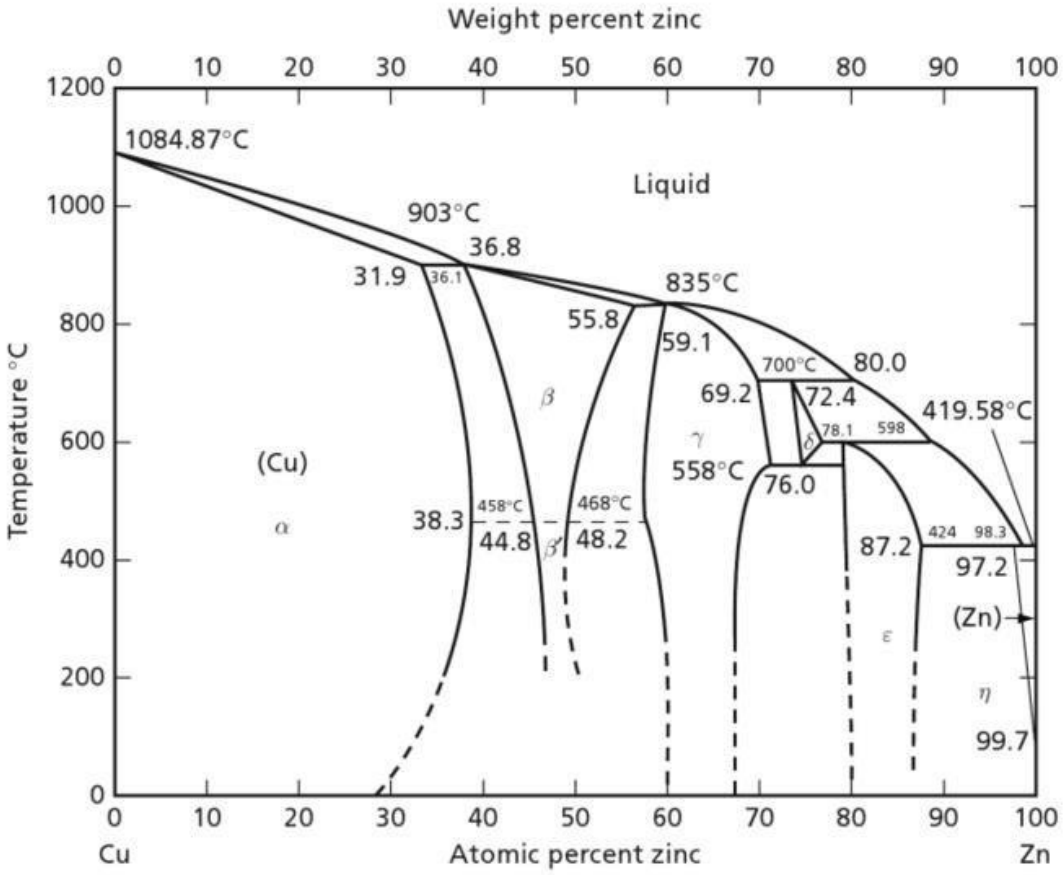

Fig 10: Phase diagram of Cu-Zn showing atomic and weight percentages of Zn [28]

The sample used in this research is rich in Cu. It can be observed from fig 10 that α- brass has

less than 35 at% Zn. βl phase is observed when 35-45 at% Zn is present and below 460°C approximately. α- brass is used in the sample in this research.

1.9 Uphill diffusion

Almost all the elements diffuse from regions of higher concentration to lower concentrations. This diffusion is well known as downhill diffusion. But the presence of substitutional and interstitial elements in an alloy and their kinetic behaviors can cause uphill diffusion i.e. the diffusion of elements against their concentration. Liu et al [29] in their work on Fe-Mn-C diffusion couple demonstrated that presence of Mn increased the activity (chemical potential) of C, because of which it diffused uphill. Nishibata et al [30] have done kinetic analysis of uphill diffusion of carbon in low carbon steels. Zhang [31] reported the uphill diffusion of Cu in Al-Si-Cu-Mg alloys. Dung [32] reported the uphill diffusion of Si interstitial during Boron diffusion in Si. A concentration profile showing the concentrations of Si and B can be seen in fig 11. Which clearly shows the increase in concentration of Si.

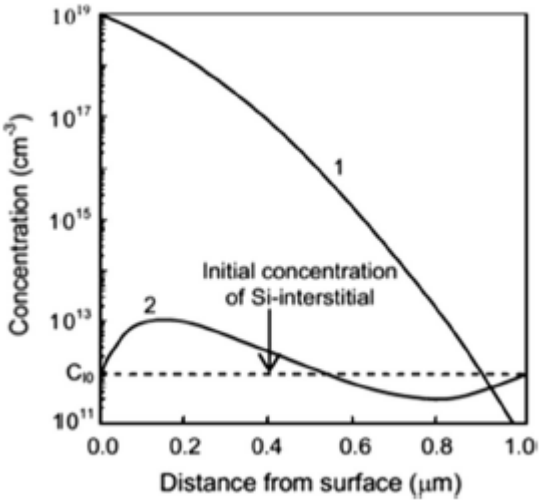

Fig 11: Concentration profiles of Boron (curve 1) and Si (curve 2) for 10 minutes of diffusion at 1000°C[32]

L. S. Darken in his work [33] mentioned that ‘‘for a system with more than two components it is no longer necessarily true that a given element tends to diffuse toward a region of lower concentration even within a single-phase region’’

‘‘The driving force in an isothermal diffusion process may be regarded as the gradient of the chemical potential’’, and

‘‘departure from the behavior of an ideal solution may be so great that the concentration gradient and the chemical potential gradient, or activity gradient, may be of different sign, thus giving rise to uphill diffusion’’.

In his experiment, to show diffusion of carbon in two austenite bars of two different compositions, Darken proved that carbon diffused from low concentration to high concentration.

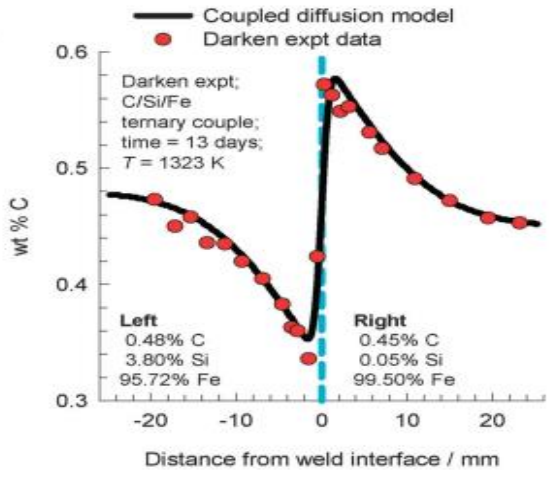

Fig 12: Inter diffusion between austenite bars with different compositions showing uphill diffusion [34]

1.10 Kirkendall Voids

As mentioned earlier that diffusion happens through vacancy mechanism. So, when atoms move in a direction there will be flow of vacancies in opposite direction. If the diffusion happens by ring or exchange mechanism, the rate of diffusion of elements on both the sides should be equal.

When a hypothetical diffusion couple is created with an inert marker placed at the junction, and diffusion is allowed to happen, it can be observed that the inert marker moves towards material having greater diffusion flux i.e. in the direction of slowest moving component.

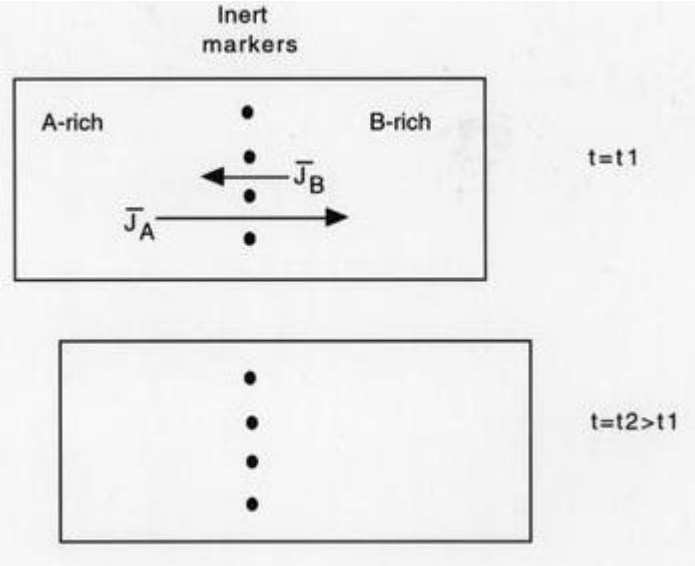

Fig 13: Schematic of a diffusion couple with diffusion fluxes JA>JB showing movement of marker towards A rich side because of greater diffusion flux [35]

When atoms from both sides of diffusion couple diffuse, the vacancies from both the sides move and they get coalesced at the interface. These vacancies form as voids. These voids are called as kirkendall voids. Kirkendall voids are common in diffusion couple. They are also observed in microelectronics research because of growth of IMC due to electromigration in solder bumps [36][37][38][39].

As mentioned earlier, one of the components in diffusion couple loses while other gains mass because of difference in diffusivity. The side which loses mass experiences tensile stress, while that gains mass experiences compressive stresses. The flow of vacancies along with these stress leads to the formation of voids.

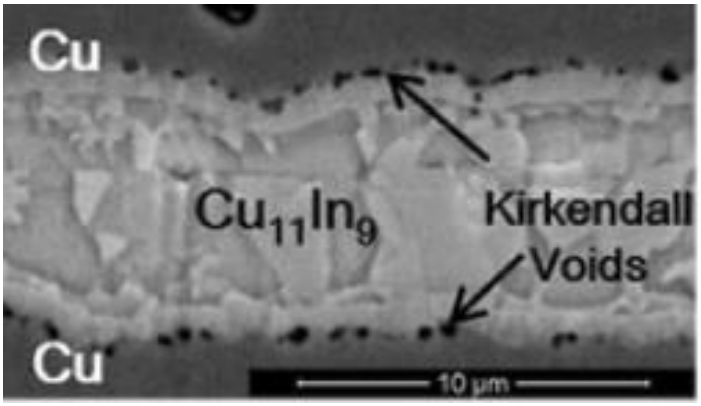

Fig 14: Kirkendall voids seen at the interface of Cu-In diffusion couple [38]

As the diffusion continues, these kirkendall voids will be coalesced and grow into a crack. When the crack is formed as shown in fig 15, the diffusion across the IMC interfaces stop.

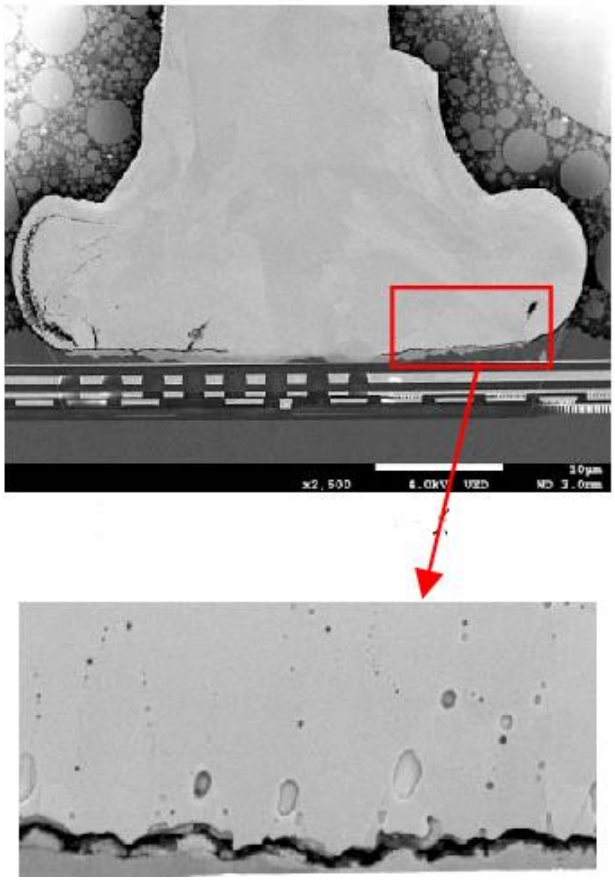

Fig 15: Crack growth in copper wire bond pad [40]

CHAPTER 2

DIFFUSION AND GROWTH OF INTERMETALLIC COMPOUNDS

2.1 Experimental Procedure:

2.1.1 Preparation of three-layered Brass-Al bimetal

As received material, three layered Brass-Aluminum bimetal consists of Aluminum 5xx in between two layers of α-Brass (70 at% Cu & 30 at% Zn). The thickness of the sheet is

approximately 1.3mm. The bimetal sheets are made using roll bonding. During a cold roll bonding, the sheets that are being subjected to bonding are cleaned and are scratched in order to increase the coefficient of friction. The sheets are then passed through rollers, with adequate pressure. Thus, a clad metal sheet is obtained with reduced combined thickness. This rolled bimetal is further subjected to heat treatment for better adhesion of layers.

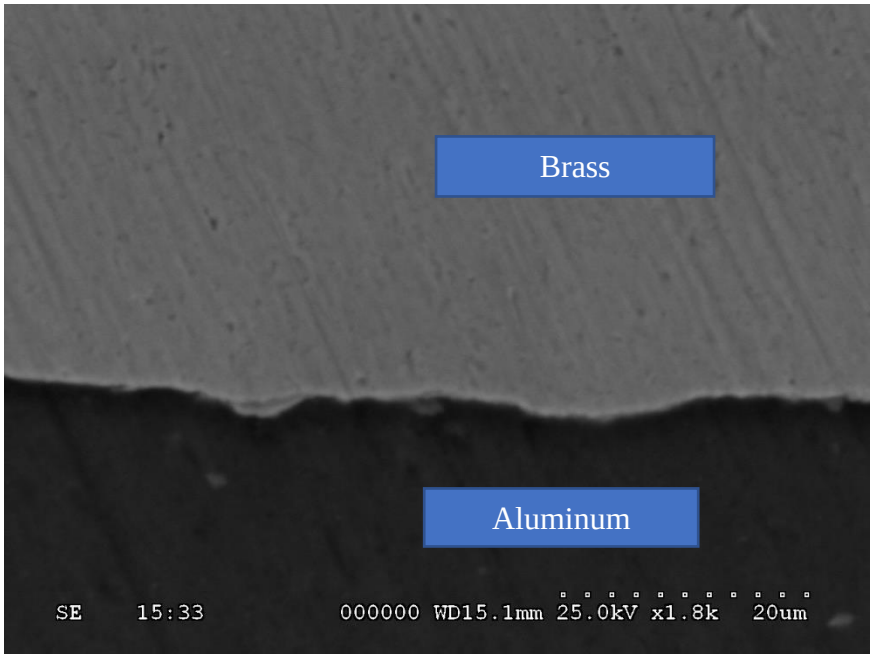

Figure 16: Secondary Electron Image of sample before Annealing

A bimetal strip generally consists of two different metallic layers. Different metals have different coefficient of thermal expansion. When a bimetal strip is subjected to heat, it bends in the direction of metal with low coefficient of expansion. Since the interest of our study is diffusion, the bimetal is subjected to heat treatment, which can bend or delaminate it. Therefore, a three-layered bimetal is used in this study.

All the samples, 10 mm X 10 mm (approximately) are cut from as received material using a

rotary cutting tool carefully. These samples are subjected to annealing in a tube furnace at different temperatures (350°C, 400°C) for different lengths of times. The heat-treated samples are then put in a mold and a thermosetting resin is poured. This resin is left for 12 hours to set. This whole process is called resin casting.

2.1.2 Annealing of samples in a tube furnace

As mentioned earlier, annealing heat treatment is a process in which a metal sample is heated above the recrystallization temperature for certain amount of time and left to cool in the air. Heat treatment of material is done either to reduce internal stresses or to change physical/chemical/mechanical properties.

In this study, samples are heat treated at 350°C and 400°C in a tube furnace. A tube furnace consists of a glass tube in which sample can be placed. This glass tube is placed in a hollow horizontal cylindrical chamber which produces heat. To avoid oxidation of metal during heat treatment, both the ends of glass tube of the furnace are closed, and the glass tube is circulated with Argon gas to create inert atmosphere.

2.1.3 Resin Casting (Mounting)

The area of interest in our samples is the cross section of the heat-treated sample. The thickness of the sample is about 1.3 mm. Since it is hard to hold a sample with such small thickness to polish, the sample is made to stand in a mold and a mixture of resin and hardener is poured. The mixture filled mold is then allowed to set (harden). It will be hard to remove a hardened resin casted sample from a mold, because of the sample sticking to walls of the mold. To avoid such sticking, the walls of mold are lubricated prior to the pouring of resin and hardener mix. After the sample is set, it can be easily removed from the mold, as the walls of mold are lubricated. The

sample is now big enough to handle to grind and polish. Any excess resin from hardened sample can be removed by grinding.

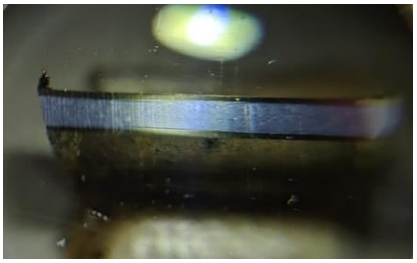

Figure 17: A top view of resin casted (mounted) sample

2.1.4 POLISHING

As the thickness of sample is very small, the samples should be carefully polished to avoid scratches. All the samples in this research are manually prepared (polished). In order to make sure that the scratches from previous polishing direction is removed, the sample is rotated 90 degrees for further polishing. After the process of intermediate polishing, the sample is polished polishing wheel covered with a smooth cloth that is charged with abrasive particles. A wide range of abrasive materials are used for different materials to be polished. In this study, 1μm alumina and 0.05μm alumina powders are used. The sample should be finely polished to study under optical and electron microscopes.

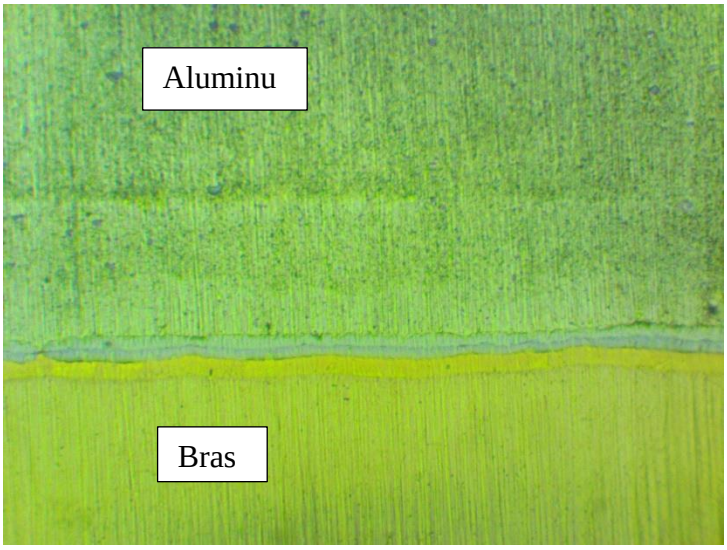

Fig 18: Optical microscope image of sample after fine polishing

2.1.5 SPUTTERING

It is a vacuum deposition method used to deposit or coat a layer of metal or alloy on a specimen to prevent the nonconductive specimen in an SEM chamber (high voltage, high vacuum) from charging effect.

Ion beam sputtering is a type of sputtering in which an ionized gas is used to hit a target to remove the ions from it. These removed ions are deposited onto the substrate (specimen). Argon is used as ionization gas and carbon is used as target material in this study.

Though the sample is finely polished, charging effect was observed on the sample under SEM. Charging effect is caused by accumulation of static charges over sample surface. This is because the resin used to mold the sample is nonconductive. Therefore, the resin part of sample surface is covered using copper and carbon tape. Also, the sample is coated with thin layer of carbon using sputtering.

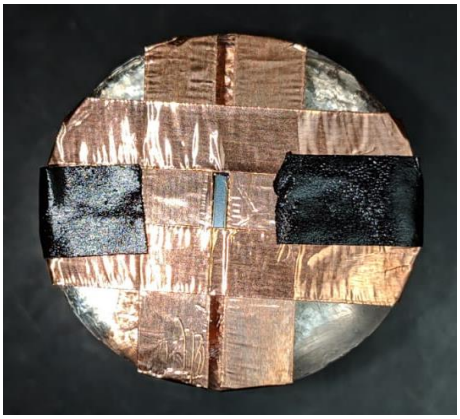

Fig 19: Sample surface covered with copper and carbon tapes and coated with thin layer of carbon

2.1.6 Scanning Electron Microscopy

One of the objectives of our research is to find the growth (thickness) of IMC layers. Since the IMC layers are in micrometer range, they can be analyzed using Scanning Electron Microscope (SEM). A SEM produces a focused electron beam which upon hitting the sample surface produces image of the sample. The electron generated from electron source is called primary electron. Different lenses are used to focus this electron beam on to the surface of the sample. When these primary electron beam hit the sample surface, secondary electrons from sample surface are produced and are detected using a secondary electron detector, which gives a secondary electron image (SEI). The primary electrons are scattered back and can be detected by back scattered electron (BSE) detector.

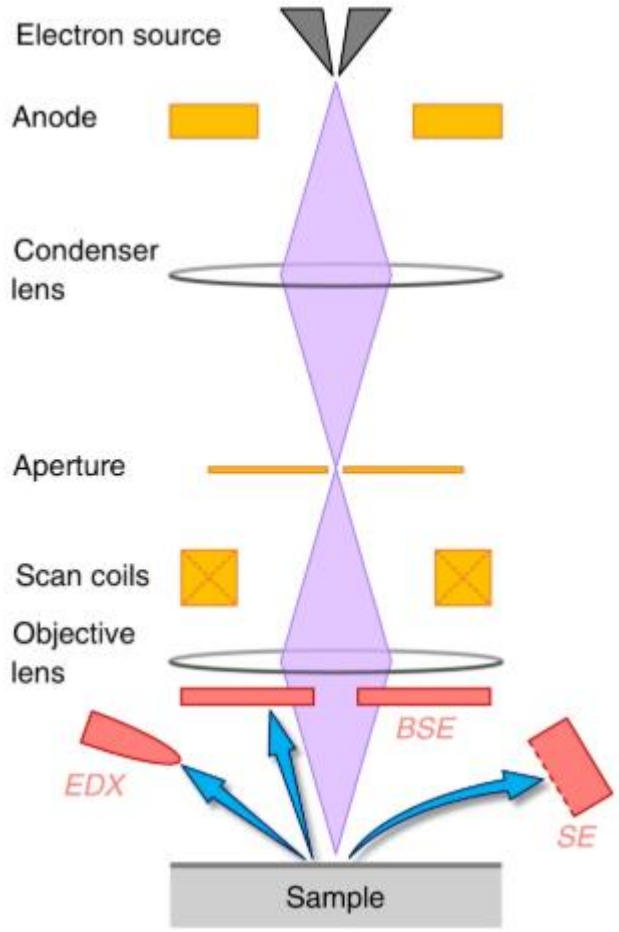

Fig 20: Schematic of Scanning Electron Microscope [41]

SE Image is useful for studying topography while BSE Image is useful for the study of atomic number of materials based on the brightness. Higher the brightness of material, higher is their atomic number. Because of the clear contrast that can be observed in between intermetallic compounds, the area of each IMC can be found using a software Image J.

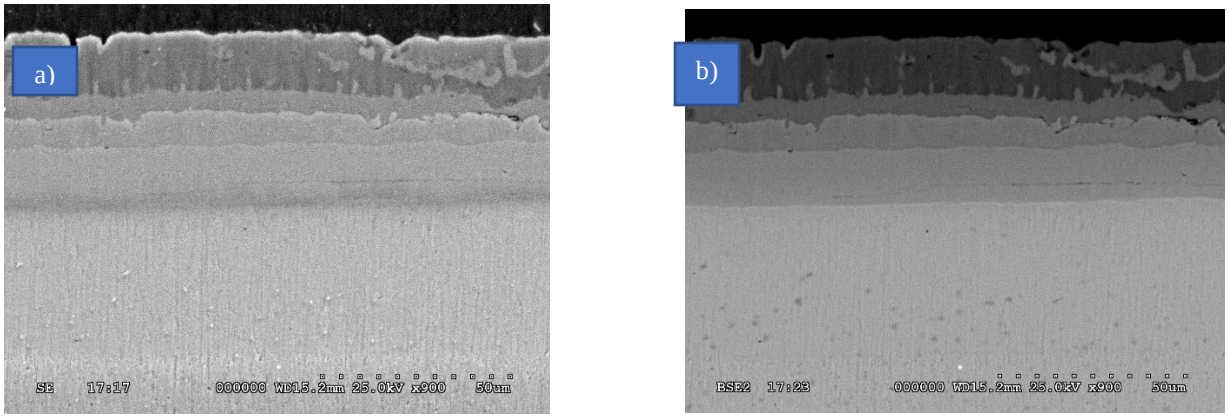

Fig 21: a) Secondary Electron (SE) and b) Back Scattered Electron (BSE) images of same sample heat treated at 400°C for 20 hours

As the secondary electrons are knocked out of their orbitals, the electrons from neighboring orbitals jump to occupy the lower energy levels releasing energy. This energy is released in form of x-rays. Each element has its own characteristic x-ray. Thus, energy dispersive x-ray spectroscopy (EDS/EDX) can produce results showing the element present at the spot of analysis.

2.2 Results

As received sample of Brass and Aluminum bimetal is finely polished and is studied under optical microscope.

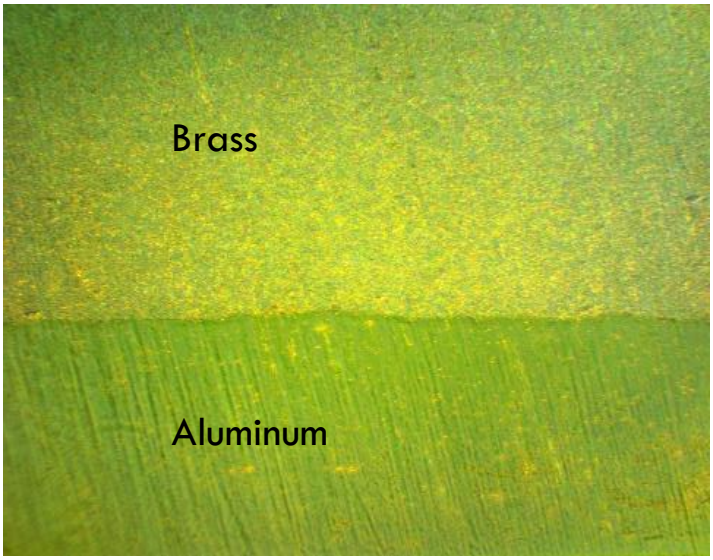

Fig 22: Optical Microscope image of sample before heat treatment

SEM image of sample before heat treatment was taken and EDS analysis was performed to find the composition.

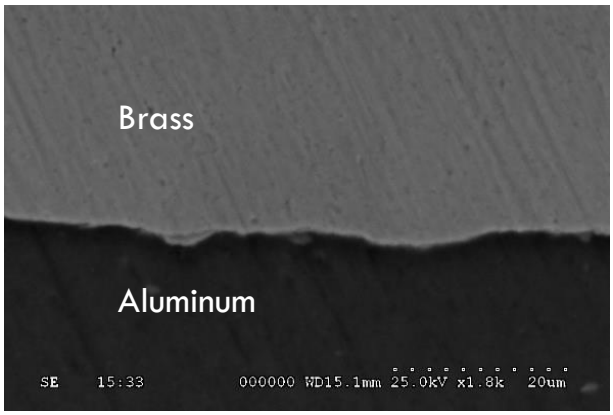

Fig 23: SEM image of sample before annealing

Aluminum - 98.46 at% of Al and 01.53 at% of Mg

Brass - 69.53 at% of Cu and 30.46 at% of Zn

The samples were later subjected to annealing heat treatment at 350°C and 400°C and soaked for different amounts of times. The samples were then taken out of furnace and mounted to polish. The polished samples were studied under optical microscope and SEM.

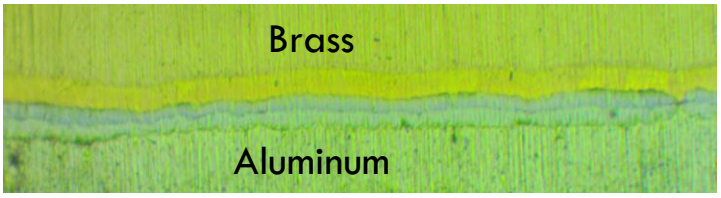

Fig 24: Formation of IMC as observed in optical microscope image post annealing

The optical microscope image of sample after heat treatment shows three distinct layers formed in between brass and aluminum. One of the layers formed is inside brass. So the sample is further studied under SEM. SEM Images of samples annealed at 350 and 400°C for different lengths of time are shown in fig 25-29.

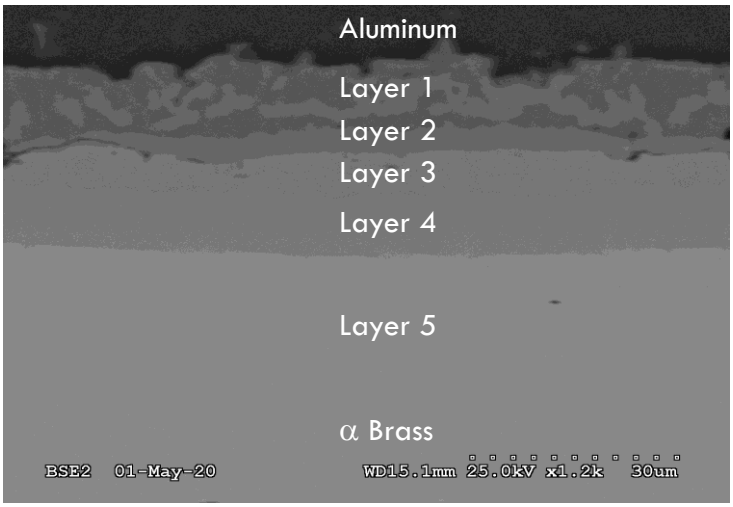

Fig 25: SEM image of sample annealed at 350°C for 44 hours

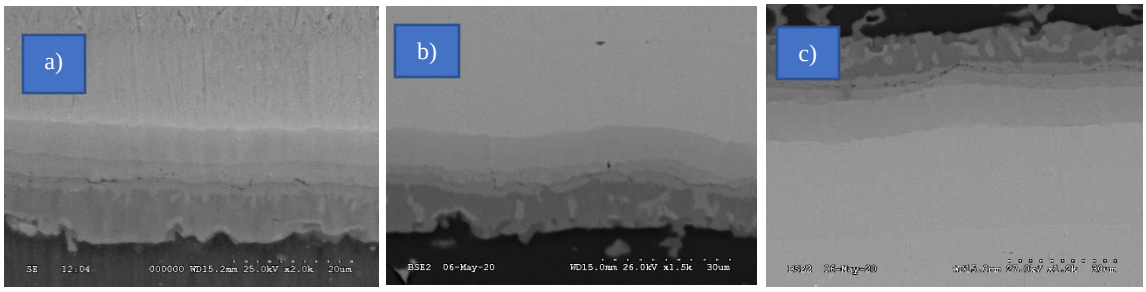

Fig 26: Samples annealed at 350° C for a) 9 hours b) 26 hours c) 54 hours

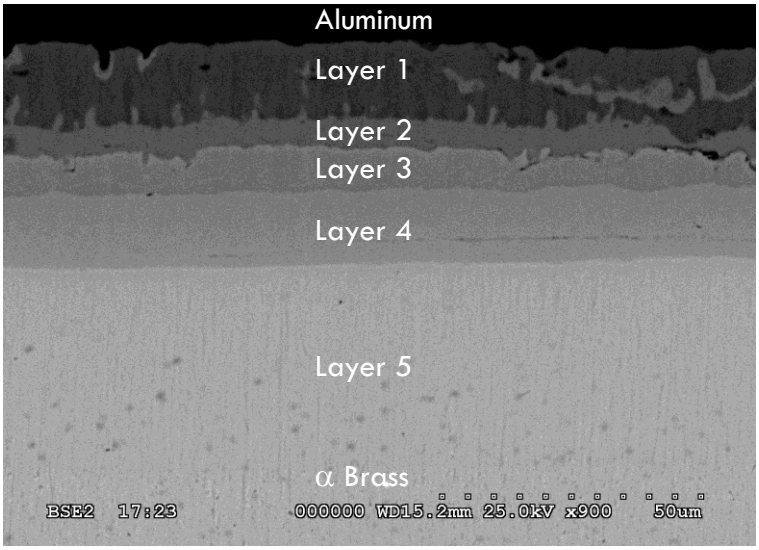

Fig 27: SEM image of sample annealed at 400°C for 20 hours

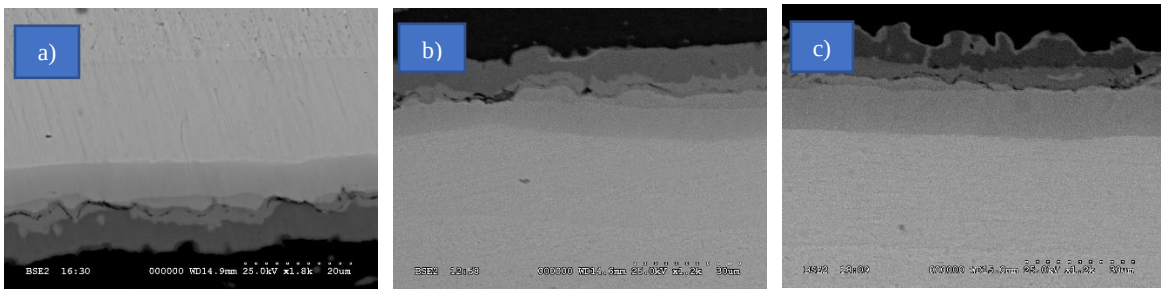

Fig 28: SEM Images of samples annealed at 400°C for a) 2 hours b) 5 hours c) 9 hours

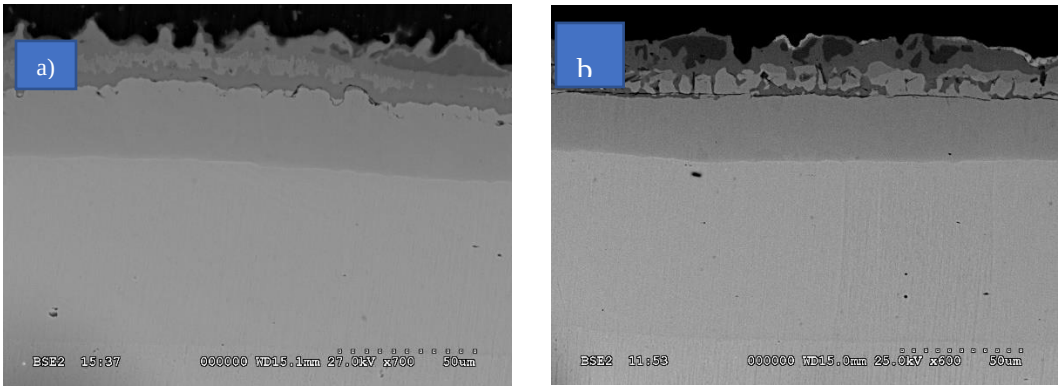

Fig 29: SEM Images of annealed samples at 400°C for a) 44 hours b) 54 hours

2.3 Observations

Dark side of the sample is Aluminum and bright side is Brass. All the samples annealed at 350°C have 5 layers of IMC's formed between Al and Brass and are named layer 1-5 from Al side to Brass side. Kirkendall voids are observed in between layers 2 and 3. Samples annealed at 400°C for 2,5,9 & 20 hours also have 5 IMC layers. But the samples annealed at 400°C for more than 20 hours i.e. for 44, 54 hours do not have distinct layers on Al side (layers 1&2 are not distinct).

CHAPTER 3

DETERMINATION OF INTER METALLIC COMPOUNDS

3.1 Experimental Procedure

3.1.1 EDS Analysis of samples

EDS analysis is used to find elements and their proportions in a sample. Initially EDS is done on entire sample image area which can be called as EDS area scan. This area scan gives x-ray spectrum from entire area. It also defines the elements present in the sample.

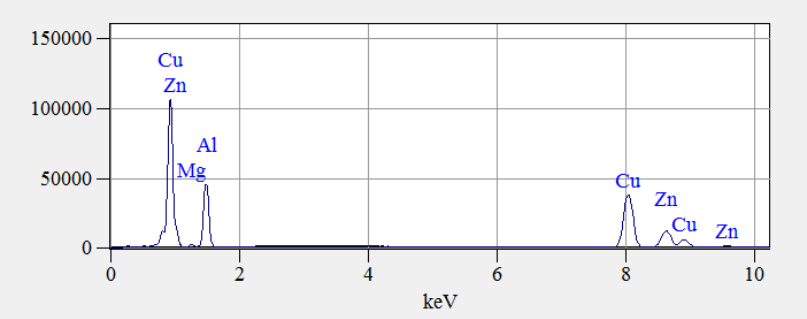

Fig 30: X-ray spectra of the entire sample image area of sample annealed at 400°C for 20 hours

EDS line scan is done to plot the relative proportions of previously identified elements in IMC's. The resulting EDS line scan analysis is shown in fig 31.

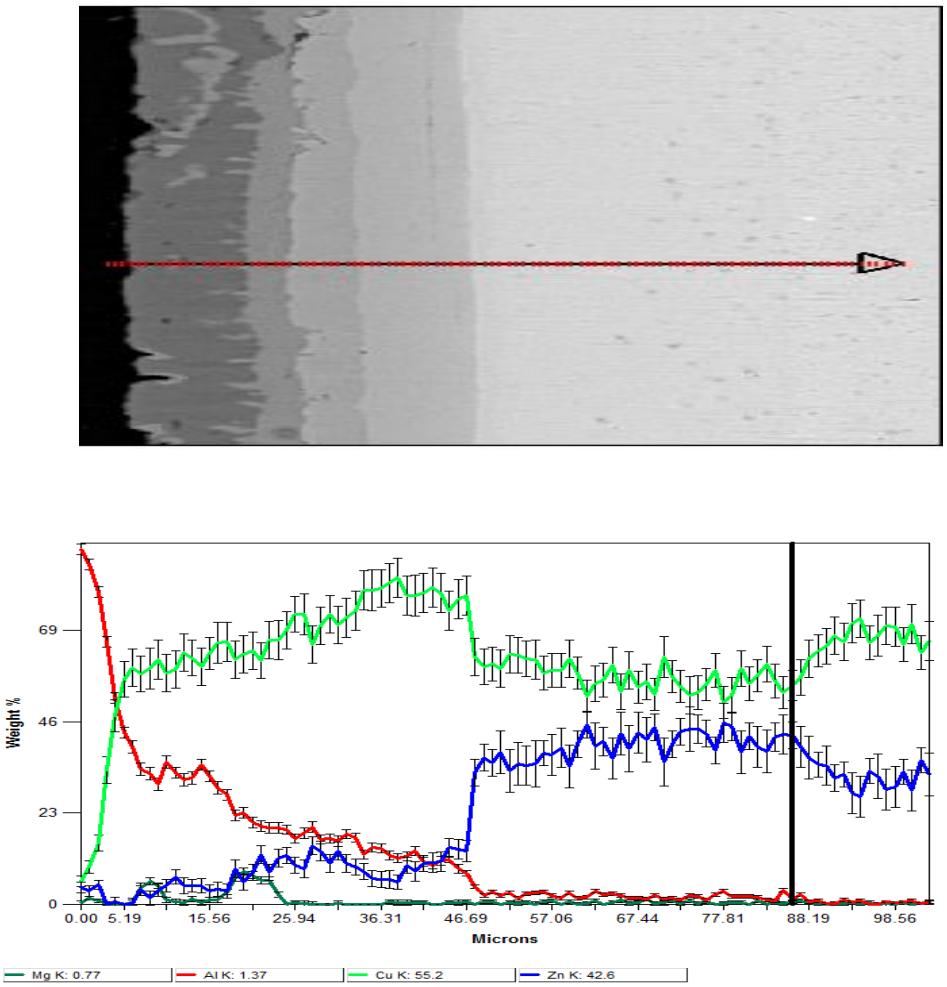

Fig 31: EDS line scan of annealed sample at 400°C for 20 hours

EDS spot analysis is done to know atomic percentage or weight percentage of element present at that spot.

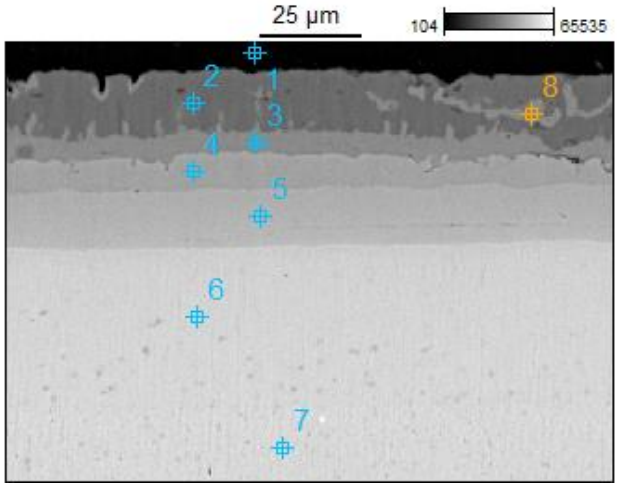

	Mg at%	Al at%	Cu at%	Zn at%
pt1	0.82	95.82	1.74	1.62
Pt2	0.34	60.27	38.76	0.62
Pt3	9.10	36.74	49.69	4.48
Pt4	0.43	33.11	58.78	7.69
Pt5	0.36	25.69	67.53	6.42
Pt6	0.00	4.35	59.06	36.59
Pt7	0.63	1.42	67.81	29.84
pt8	0.94	58.63	39.32	1.11

Fig 32 & Table 1: EDS spot analysis of sample annealed at 400°C for 20 hours

3.2 EDS Spot Analysis Results

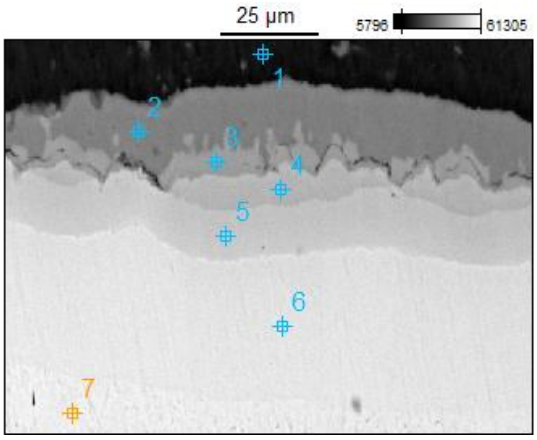

	Mg at%	Al at%	Cu at%	Zn at%
pt1	1.17	95.70	1.64	1.49
Pt2	0.26	61.99	37.27	0.47
Pt3	9.84	36.99	49.05	4.12
Pt4	0.45	35.01	57.45	7.09
Pt5	0.46	24.11	68.55	6.87
Pt6	0.00	3.34	58.73	37.92
Pt7	0.55	0.61	69.36	29.47

Fig 33 & Table 2: EDS spot analysis of sample annealed at 400°C for 2 hours

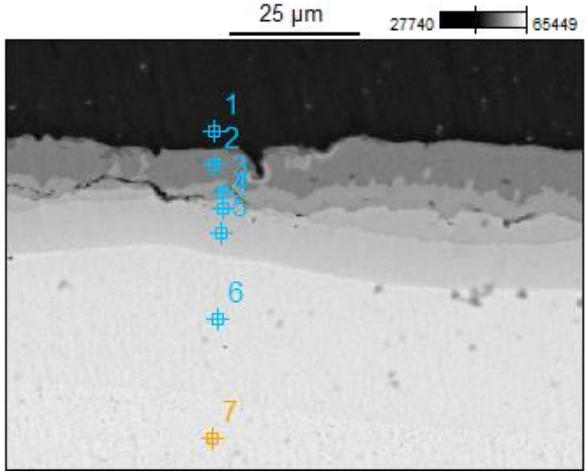

	Mg at%	Al at%	Cu at%	Zn at%
pt1	0.90	95.35	2.05	1.70
Pt2	0.52	63.28	35.37	0.83
Pt3	10.06	37.39	47.88	4.67
Pt4	0.34	35.44	58.53	5.69
Pt5	0.39	24.94	67.58	7.09
Pt6	0.00	4.23	58.47	37.30
Pt7	0.66	9.29	62.71	27.35

Fig 34 & Table 3: EDS spot analysis of sample annealed at 400°C for 5 hours

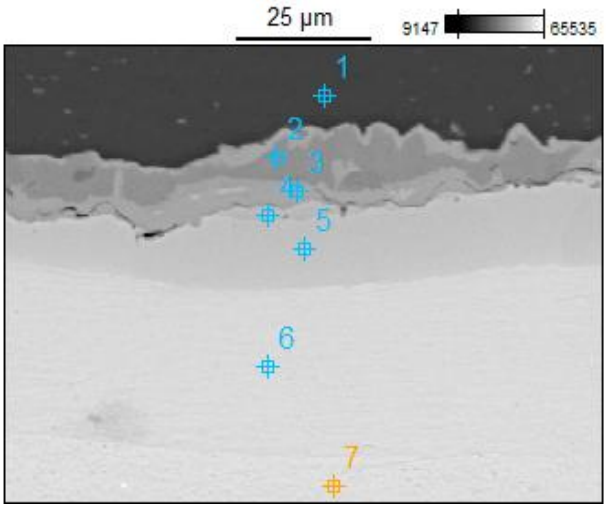

	Mg at%	Al at%	Cu at%	Zn at%
pt1	1.06	96.26	1.62	1.05
Pt2	0.62	59.36	39.17	0.84
Pt3	10.47	37.47	48.03	4.03
Pt4	3.03	34.37	55.53	7.08
Pt5	0.57	26.29	67.10	6.04
Pt6	0.00	4.45	59.46	36.09
Pt7	0.92	1.43	67.89	29.76

Fig 35 & Table 4: EDS spot analysis of sample annealed at 400°C for 9 hours

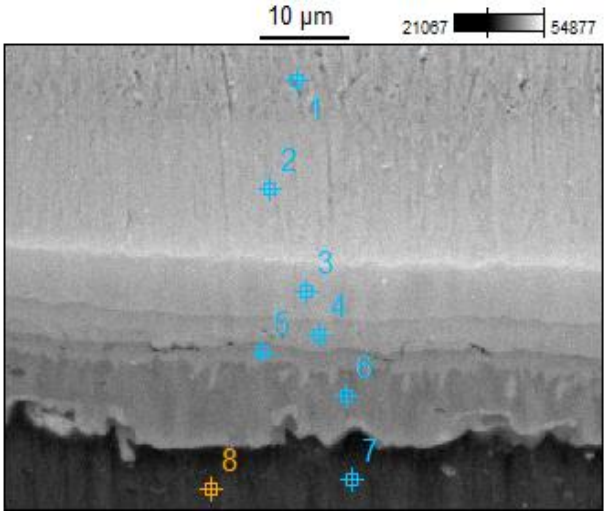

	Mg at%	Al at%	Cu at%	Zn at%
Pt1	0.27	1.16	67.45	31.13
Pt2	0.00	2.02	58.68	39.31
Pt3	0.24	17.03	75.19	7.54
Pt4	0.74	24.35	69.76	5.15
Pt5	3.69	31.21	60.81	4.29
Pt6	0.46	46.68	51.52	1.34
Pt7	0.72	96.23	1.61	1.44
pt8	0.73	96.61	1.48	1.19

Fig 36 & Table 5: EDS spot analysis of sample annealed at 350°C for 9 hours

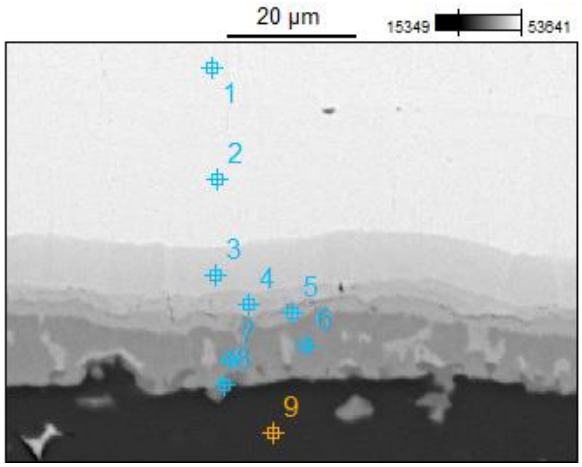

	Mg at%	Al at%	Cu at%	Zn at%
Pt1	0.166	0.193	69.229	30.411
Pt2	0.000	1.924	58.587	39.490
Pt3	0.119	14.793	77.611	7.477
Pt4	0.098	21.820	69.468	8.614
Pt5	4.785	22.556	66.464	6.194
Pt6	0.049	45.578	53.799	0.574
Pt7	0.178	45.904	53.178	0.740
Pt8	6.996	40.983	50.803	1.218
Pt9	0.487	96.372	1.662	1.480

Fig 37 & Table 6: EDS spot analysis of sample annealed at 350°C for 26 hours

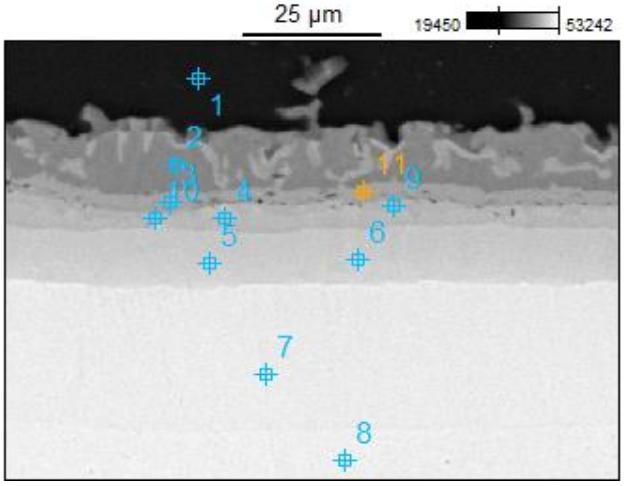

	Mg at%	Al at%	Cu at%	Zn at%
pt1	0.82	95.82	1.74	1.62
Pt2	0.34	60.27	38.76	0.62
Pt3	9.10	36.74	49.69	4.48
Pt4	0.43	33.11	58.78	7.69
Pt5	0.36	25.69	67.53	6.42
Pt6	0.00	4.35	59.06	36.59
Pt7	0.63	1.42	67.81	29.84
pt8	0.94	58.63	39.32	1.11

Fig 38 & Table 7: EDS spot analysis of sample annealed at 350°C for 44 hours

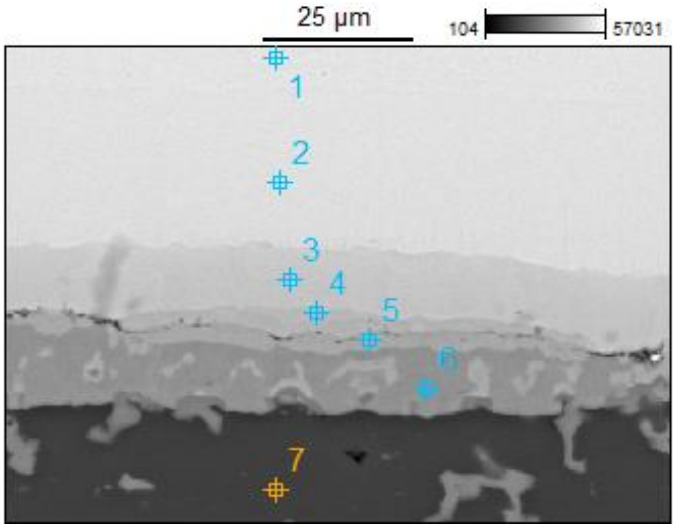

	Mg at%	Al at%	Cu at%	Zn at%
pt1	0.000	0.231	69.302	30.468
Pt2	0.000	2.275	59.679	38.047
Pt3	0.066	15.854	76.724	7.357
Pt4	0.072	20.577	70.834	8.517
Pt5	4.666	23.459	66.541	5.333
Pt6	0.038	44.839	54.490	0.633
Pt7	0.512	96.731	1.429	1.327

Fig 39 & Table 8: EDS spot analysis of sample annealed at 350°C for 54 hours

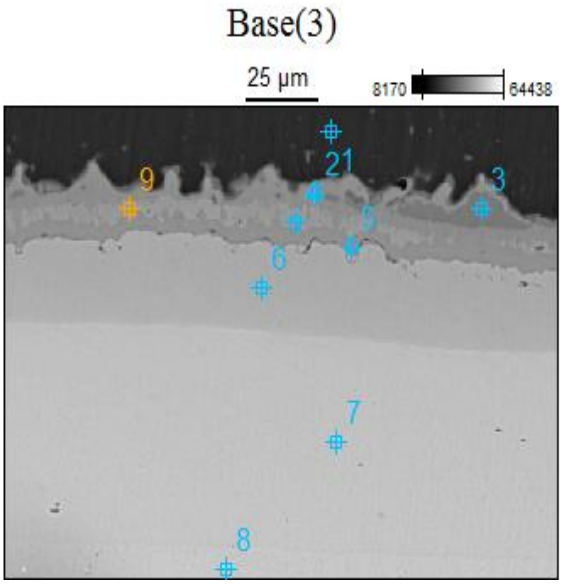

	Mg at%	Al at%	Cu at%	Zn at%
Pt1	1.04	95.82	1.91	1.23
Pt2	5.98	36.91	53.68	3.43
Pt3	0.00	49.47	49.74	0.52
Pt4	0.11	28.44	66.43	5.01
Pt5	5.94	23.54	64.23	6.29
Pt6	0.23	15.14	77.23	7.40
Pt7	0.00	2.46	60.87	36.67
Pt8	0.39	0.77	68.31	30.53
Pt9	0.80	32.80	61.46	4.94

Fig 40 & Table 9: EDS spot analysis of sample annealed at 400°C for 44 hours

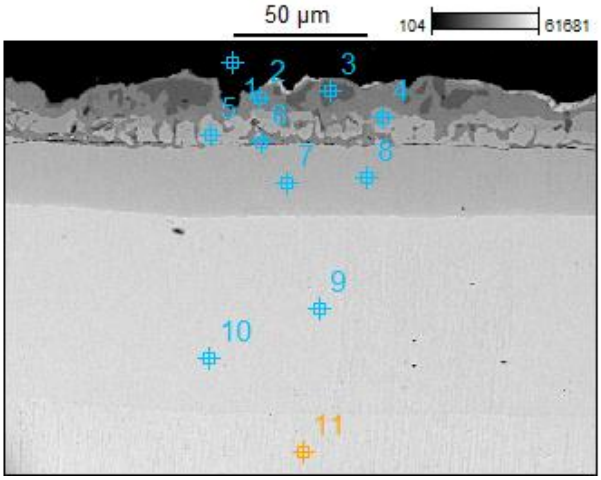

	Mg at%	Al at%	Cu at%	Zn at%
pt1	1.11	95.69	1.97	1.23
Pt2	7.54	30.33	58.75	3.38
Pt3	0.15	53.00	46.31	0.54
Pt4	0.47	24.97	67.89	6.68
Pt5	0.42	19.59	74.50	5.49
Pt6	0.87	19.45	73.46	6.22
Pt7	0.30	15.78	75.16	8.77
Pt8	0.26	16.19	74.90	8.66
Pt9	0.00	3.05	61.01	35.95
Pt10	0.00	2.50	60.50	36.99
pt11	0.35	0.47	68.96	30.22

Fig 41 & Table 10: EDS spot analysis of sample annealed at 400°C for 54 hours

3.3 XRD Pattern Data Results

The sample is cut through layers 2 and 3. The sample on layer 2 side is named Al side and on layer 3 is named as Brass side and X Ray Diffraction is done.

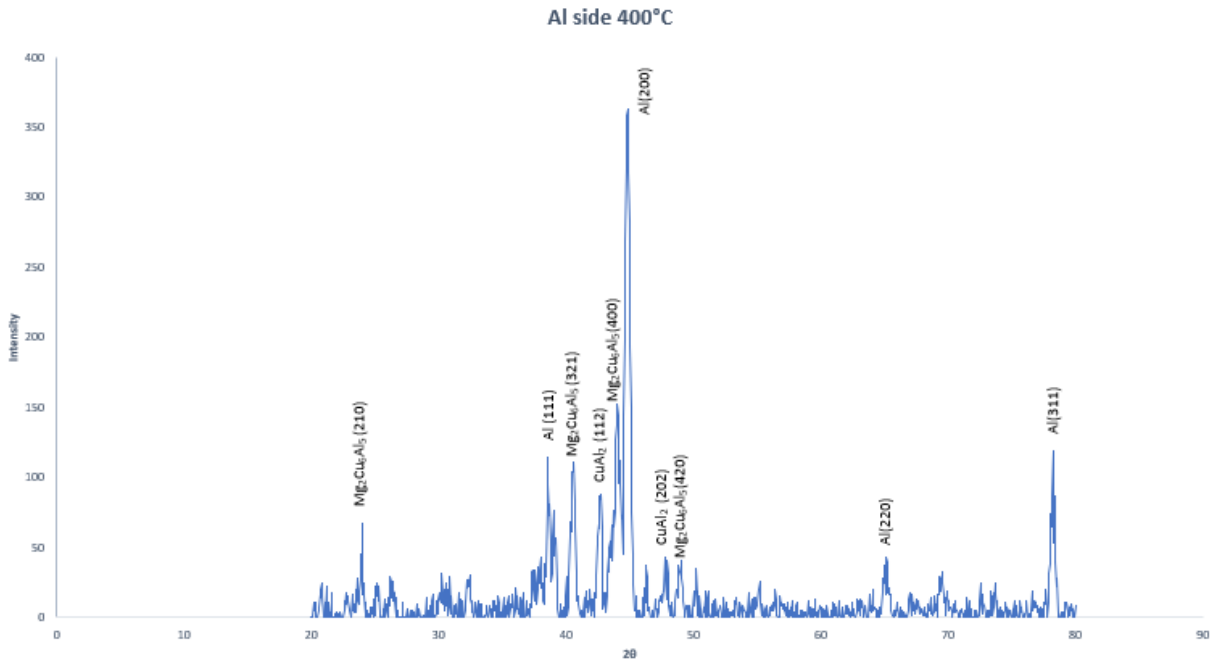

Graph1: XRD pattern showing possible IMC's on Al side of annealed sample at 400°C

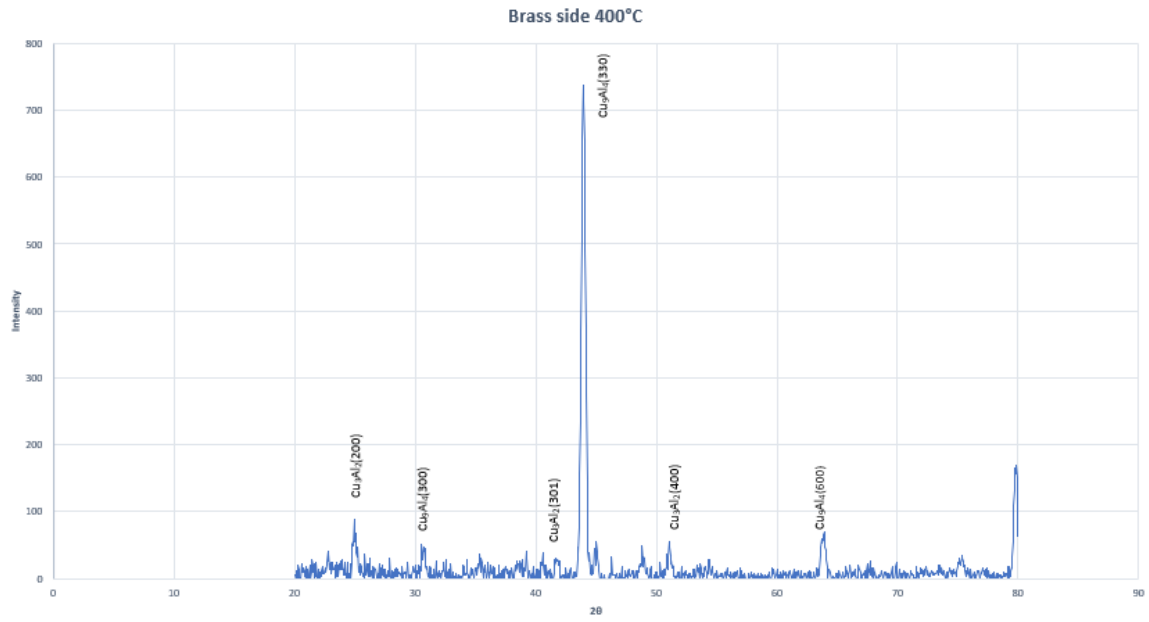

Graph 2: XRD pattern showing possible IMC's on Brass side of annealed sample at 400°C

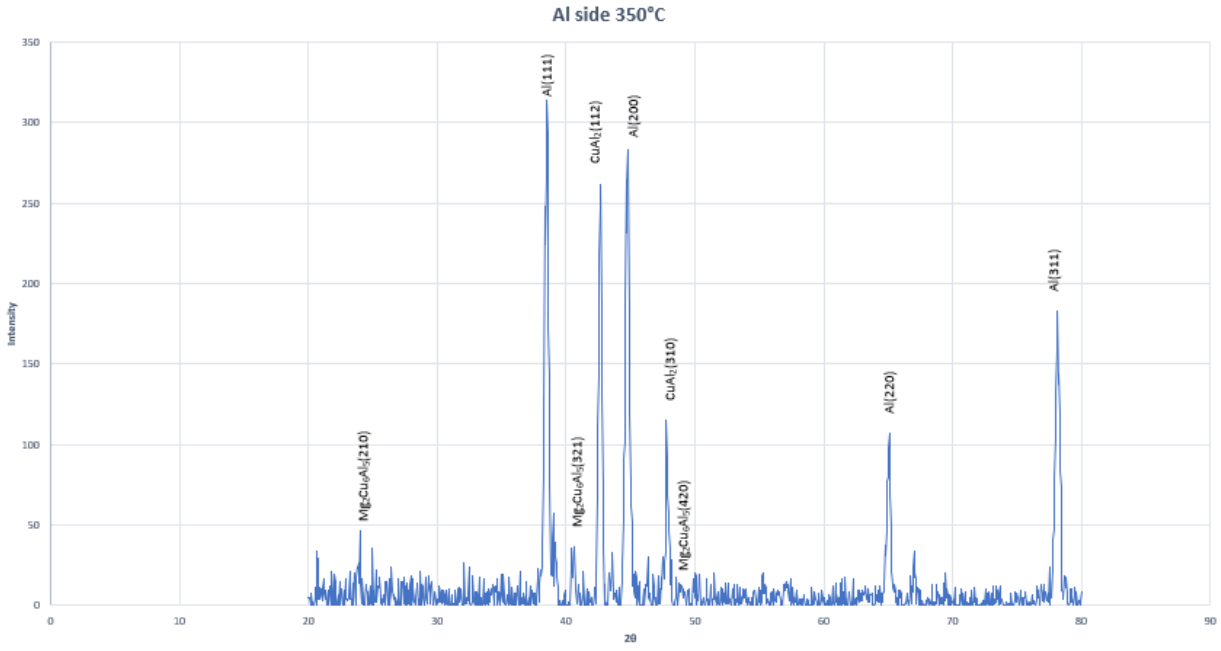

Graph 3: XRD pattern showing possible IMC's on Al side of annealed sample at 350°C

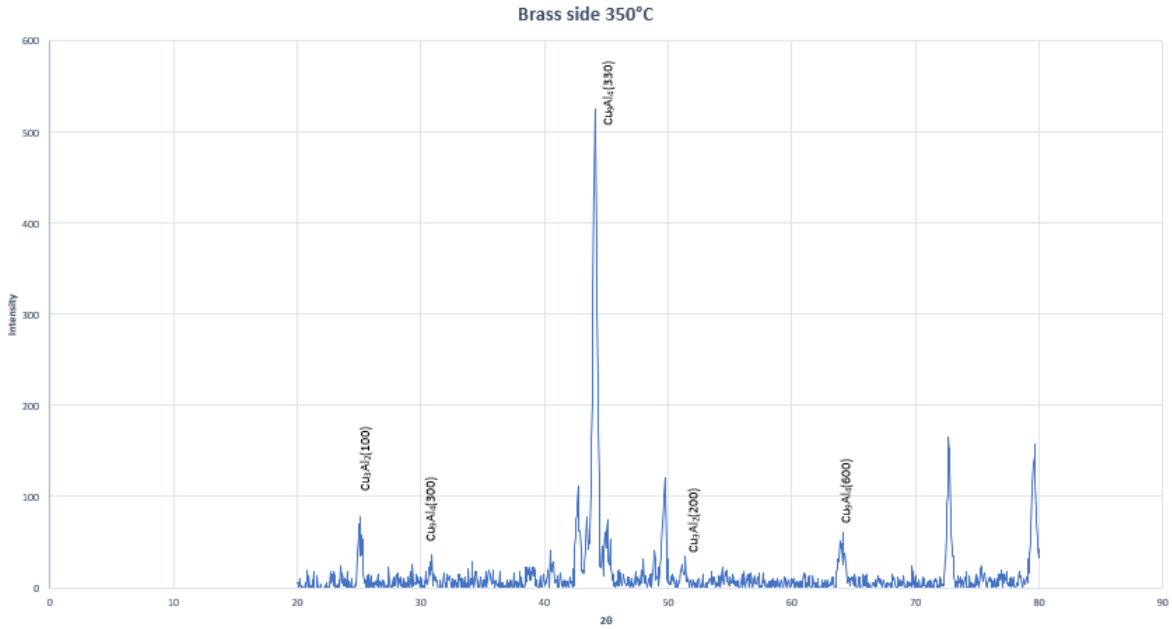

Graph 4: XRD pattern showing possible IMC's on Brass side of annealed sample at 350°C

3.4 Observations

The composition of IMC layers observed from EDS analysis, shows that they are independent of soaking time. However, the thickness of IMC's changed with respect to time as observed in [42].By comparing atomic percentages obtained from the EDS results with Cu-Al phase diagram [43]. Phases of IMC's in samples heat treated at 350 and 400°C are found to be

Layer 1 is phase θ ($CuAl_2$)

Layer 2 is $Cu_6Al_5Mg_2$

Layer 3 is δ phase (Cu_3Al_2)

Layer 4 is γ phase (Cu_9Al_4)

Layer 5 is α+ β^I (duplex brass)

CHAPTER 4

UPHILL DIFFUSION OF ZINC & MAGNESIUM

4.1 EDS Mapping results of samples & Observations

When primary electron from electron gun hits the sample surface, characteristic x-rays from the elements present in the sample are detected by EDX detector. The EDS mapping shows the presence of elements in particular area of the sample.

When EDS mapping of all the heat-treated samples are done, all the images showed similar EDS mapping results.

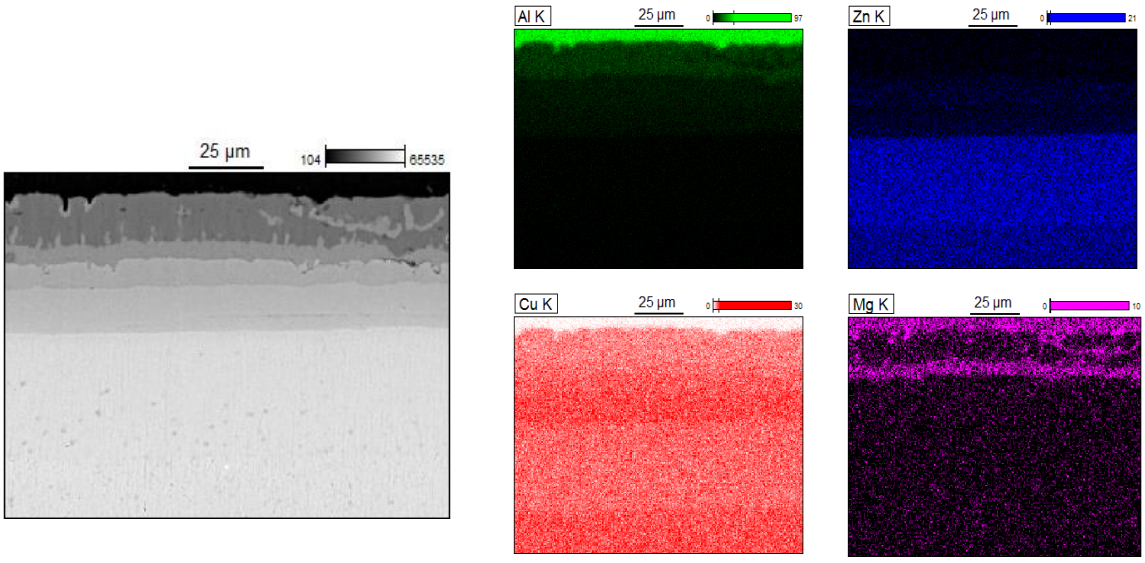

Fig 42: EDS Mapping of elements present in heat-treated samples at 350 & 400°C

From fig 40, it can be observed that zinc is enriched in layer 5 and forms duplex brass ($\alpha+ \beta^{I}$ brass) inside α-brass and Mg is enriched in layer 2 and forms $Mg_2Cu_6Al_5$.

4.2 Comparison of concentration profiles

EDS line scan data of all the samples as shown in fig 31 is compared with fig 12 showing uphill diffusion of carbon and fig 41 showing uphill diffusion of Mg.

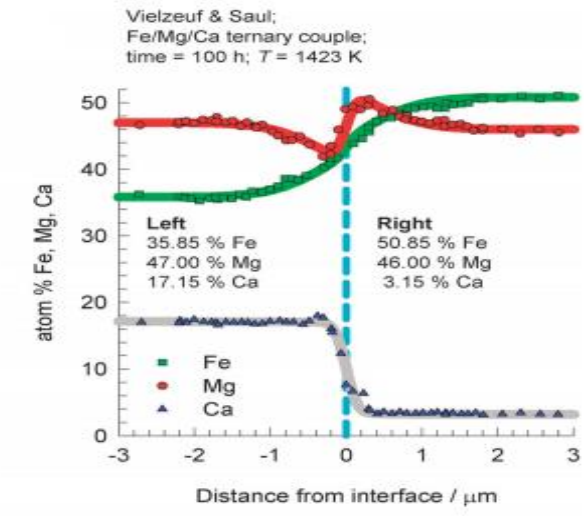

Fig 43: Inter diffusion in Fe-Mg-Ca mixture with different compositions on two sides [34]

CHAPTER 5

DETERMINATION OF INTERMETALLIC COMPOUND THICKNESS

5.1 Experimental Procedure

As mentioned earlier, one of the main objectives of this study is to find the growth rate of IMC. BSE images show good contrast difference for each IMC's. Using Image J software, the part consisting of IMC is cut and its area is calculated. The area of IMC's is then divided with the length of IMC. This gives average thickness of IMC's

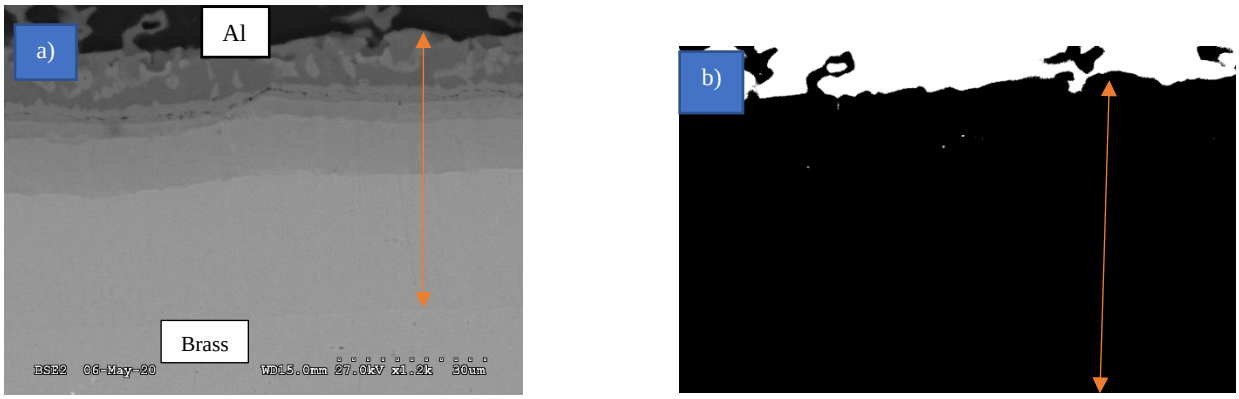

Fig 44: a) BSE image of sample and b) threshold image of sample taken in image j software

The dark area observed in the image next to BSE image gives the total area of IMC's and duplex brass layers. This dark area (threshold) is selected from the software based on the contrast difference. All the area in BSE image with different contrasts in between Al and Brass is selected. The total calculated area is then divided by the length to get overall diffused layers thickness.

5.2 Thickness trend analysis

The thickness values of diffusion layer of each individual sample is calculated and thickness vs square root of time graphs are drawn.

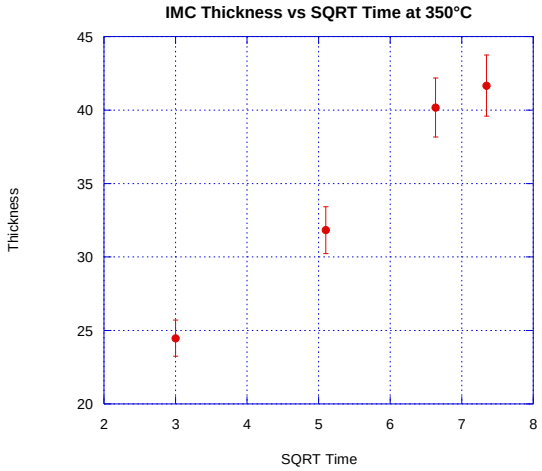

Graph 5: Thickness of IMC vs square root of time graph of samples at 350°C

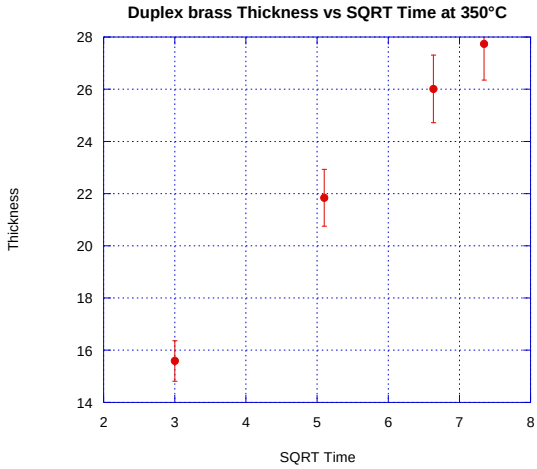

Graph 6: Thickness of duplex brass vs square root of time of samples at 350°C

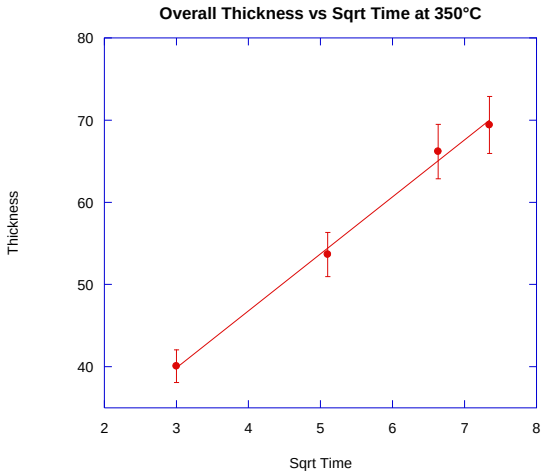

Graph 7: Overall thickness (IMC+ duplex brass) vs square root of time of samples at 350°C

	9 hours	26 hours	44 hours	54 hours
IMC (µm)	24.474	31.83	40.181	41.66
Zn rich (µm)	15.59	21.84	26.012	27.74
Overall (µm)	40.064	53.672	66.193	69.402

Table 11: Thickness values of sample at 350°C

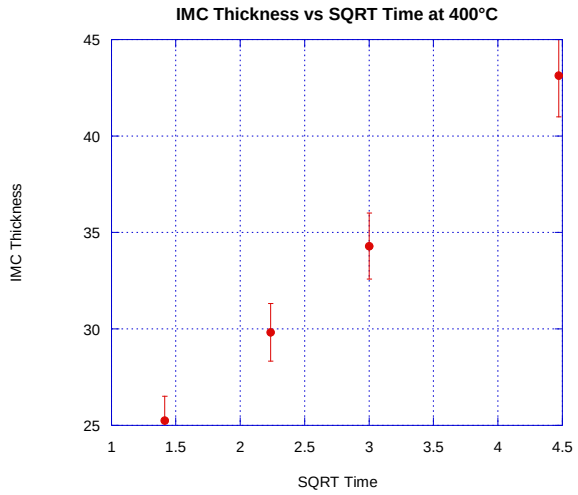

Graph 8: Thickness of IMC vs square root of time graph of samples at 400°C

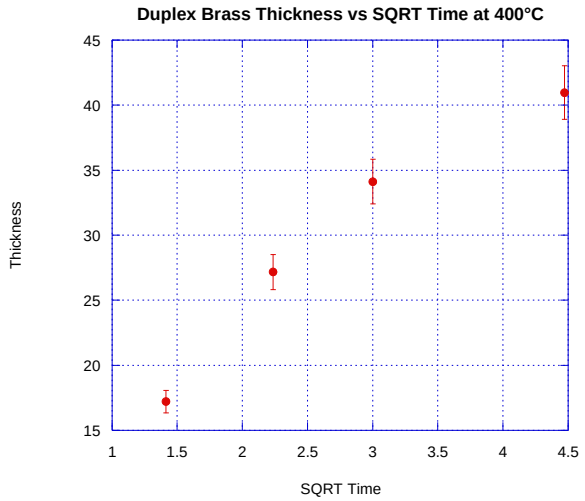

Graph 9: Thickness of duplex brass vs square root of time of samples at 400°C

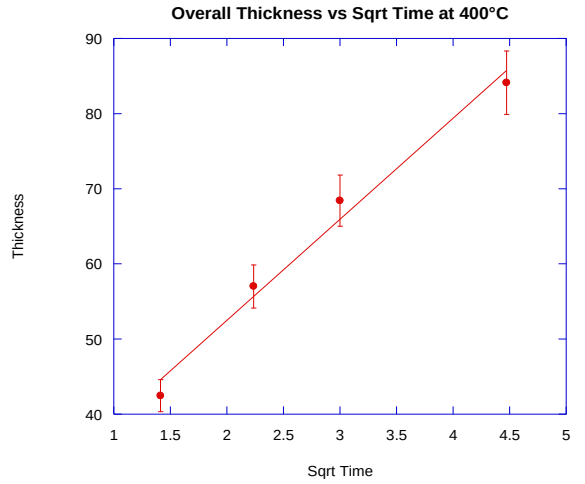

Graph 10: Overall thickness (IMC+ duplex brass) vs square root of time of samples at 400°C

	2 hours	5 hours	9 hours	20 hours
IMC (µm)	25.247	29.823	34.29	43.146
Zn rich (µm)	17.21	27.17	34.131	40.97
Overall (µm)	42.457	56.993	68.421	84.116

Table 12: Thickness values of sample at 400°C

CHAPTER 6

CONCLUSION

Different IMC's are determined by comparing the data of EDS analysis obtained, with the phase diagrams and by XRD analysis. Based on the growth rate of IMC's in all the samples, thickness is proportional to square root of time which can be given by the following equation

$x(\text{thickness}) \propto \sqrt{t}\ (\text{time})$

The growth rate follows parabolic rule as observed in [44]. Uphill diffusion of Zinc and Magnesium took place, leading to the formation of uniform layer of $\alpha+\beta^{I}$ phase adjacent to α-Brass and $Mg_2Cu_6Al_5$ adjacent to $CuAl_2$. The crack that was observed in between layers 2 ($Cu_6Al_5Mg_2$) and layer 3 (Cu_3Al_2) when sample is heat treated at 400°C for more than 20 hours is because of coalescence of kirkendall voids. This stopped the diffusion of elements across the interface.

REFERENCES

[1] D. R. Lesuer, C. K. Syn, O. D. Sherby, J. Wadsworth, J. J. Lewandowski, and W. H. Hunt, "Mechanical behaviour of laminated metal composites," *Int. Mater. Rev.*, vol. 41, no. 5, pp. 169–197, 2012, doi: 10.1179/095066096790151204.

[2] K. Gao *et al.*, "The deformation characteristics, fracture behavior and strengthening-toughening mechanisms of laminated metal composites: A review," *Metals (Basel).*, vol. 10, no. 1, 2020, doi: 10.3390/met10010004.

[3] A. A. Bykov, "Bimetal production and applications," *Steel Transl.*, vol. 41, no. 9, pp. 778–786, 2011, doi: 10.3103/S096709121109004X.

[4] W. Jiang, G. Li, Y. Wu, X. Liu, and Z. Fan, "Effect of heat treatment on bonding strength of aluminum/steel bimetal produced by a compound casting," *J. Mater. Process. Technol.*, vol. 258, no. February, pp. 239–250, 2018, doi: 10.1016/j.jmatprotec.2018.04.006.

[5] A. N. Gorban, H. P. Sargsyan, and H. A. Wahab, "Quasichemical models of multicomponent nonlinear diffusion," *Math. Model. Nat. Phenom.*, vol. 6, no. 5, pp. 184–262, 2011, doi: 10.1051/mmnp/20116509.

[6] K. Khaledi, S. Rezaei, S. Wulfinghoff, and S. Reese, "Modeling of joining by plastic deformation using a bonding interface finite element," *Int. J. Solids Struct.*, vol. 160, no. October, pp. 68–79, 2019, doi: 10.1016/j.ijsolstr.2018.10.014.

[7] M. Azimi, M. R. Toroghinejad, M. Shamanian, and L. A. I. Kestens, "The effect of strain on the formation of an intermetallic layer in an Al-Ni laminated composite," *Metals (Basel).*, vol. 7, no. 10, pp. 1–14, 2017, doi: 10.3390/met7100445.

[8] R. Jafari, B. Eghbali, and M. Adhami, "Influence of annealing on the microstructure and mechanical properties of Ti/Al and Ti/Al/Nb laminated composites," *Mater. Chem. Phys.*, vol. 213, pp. 313–323, 2018, doi: 10.1016/j.matchemphys.2018.04.001.

[9] L. Li, K. Nagai, and F. Yin, "Progress in cold roll bonding of metals," *Sci. Technol. Adv. Mater.*, vol. 9, no. 2, 2008, doi: 10.1088/1468-6996/9/2/023001.

[10] H. S. Liu, B. Zhang, and G. P. Zhang, "Enhanced plasticity of Cu-based laminated composites produced by cold roll-bonding," *Mater. Sci. Forum*, vol. 667–669, no. January, pp. 1015–1020, 2011, doi: 10.4028/www.scientific.net/MSF.667-669.1015.

[11] J. Varmazyar and M. Khodaei, "Diffusion bonding of aluminum-magnesium using cold rolled copper interlayer," *J. Alloys Compd.*, vol. 773, pp. 838–843, 2019, doi: 10.1016/j.jallcom.2018.09.320.

[12] J. Dai *et al.*, "The formation of intermetallic compounds during interdiffusion of Mg-Al/Mg-Ce diffusion couples," *J. Alloys Compd.*, vol. 619, pp. 411–416, 2015, doi: 10.1016/j.jallcom.2014.09.071.

[13] H. E. Boyer, “Heat Treating of Nonferrous Alloys,” *Metallogr. Microstruct. Anal.*, vol. 2, no. 3, pp. 190–195, 2013, doi: 10.1007/s13632-013-0074-8.

[14] H. Mehrer, “37_1259.Pdf,” *Materials Transactions, JIM*, vol. 37, no. 6. pp. 1259–1280, 1996.

[15] S. Roy, S. V. Divinski, and A. Paul, “Reactive diffusion in the Ti-Si system and the significance of the parabolic growth constant,” *Philos. Mag.*, vol. 94, no. 7, pp. 683–699, 2014, doi: 10.1080/14786435.2013.859759.

[16] V. Jindal, V. C. Srivastava, A. Das, and R. N. Ghosh, “Reactive diffusion in the roll bonded iron-aluminum system,” *Mater. Lett.*, vol. 60, no. 13–14, pp. 1758–1761, 2006, doi: 10.1016/j.matlet.2005.12.013.

[17] C. Milanese, V. Buscaglia, F. Maglia, and U. Anselmi-Tamburini, “Reactive diffusion in the system vanadium-silicon,” *Acta Mater.*, vol. 50, no. 6, pp. 1393–1403, 2002, doi: 10.1016/S1359-6454(01)00445-1.

[18] S. Sen, “A study on kinetics of CrxC-coated high-chromium steel by thermo-reactive diffusion technique,” *Vacuum*, vol. 79, no. 1–2, pp. 63–70, 2005, doi: 10.1016/j.vacuum.2005.01.009.

[19] S. Roy and A. Paul, “Growth of hafnium and zirconium silicides by reactive diffusion,” *Mater. Chem. Phys.*, vol. 143, no. 3, pp. 1309–1314, 2014, doi: 10.1016/j.matchemphys.2013.11.039.

[20] D. Naoi and M. Kajihara, “Growth behavior of Fe2Al5 during reactive diffusion between Fe and Al at solid-state temperatures,” *Mater. Sci. Eng. A*, vol. 459, no. 1–2, pp. 375–382, 2007, doi: 10.1016/j.msea.2007.01.099.

[21] Y. Muranishi and M. Kajihara, “Growth behavior of Nb3Sn layer during reactive diffusion between Cu-8.3Sn alloy and Nb,” *Mater. Sci. Eng. A*, vol. 404, no. 1–2, pp. 33–41, 2005, doi: 10.1016/j.msea.2005.05.044.

[22] T. Yamada, K. Miura, M. Kajihara, N. Kurokawa, and K. Sakamoto, “Kinetics of reactive diffusion between Au and Sn during annealing at solid-state temperatures,” *Mater. Sci. Eng. A*, vol. 390, no. 1–2, pp. 118–126, 2005, doi: 10.1016/j.msea.2004.08.053.

[23] M. Mita, M. Kajihara, N. Kurokawa, and K. Sakamoto, “Growth behavior of Ni3Sn4 layer during reactive diffusion between Ni and Sn at solid-state temperatures,” *Mater. Sci. Eng. A*, vol. 403, no. 1–2, pp. 269–275, 2005, doi: 10.1016/j.msea.2005.05.012.

[24] E. G. Wagenhuber, V. B. Trindade, and U. Krupp, “The role of oxygen-grain-boundary diffusion during intercrystalline oxidation and intergranular fatigue crack propagation in alloy 718,” *Proc. Int. Symp. Superalloys Var. Deriv.*, pp. 591–600, 2005, doi: 10.7449/2005/superalloys_2005_591_600.

[25] R. German, “No Title,” *Sinter. from Empir. Obs. to Sci. Princ.*, vol. Butterwort, 2014.

[26] C. C. Lee, P. J. Wang, and J. S. Kim, “Are intermetallics in solder joints really brittle?,” *Proc. - Electron. Components Technol. Conf.*, pp. 648–652, 2007, doi: 10.1109/ECTC.2007.373866.

[27] U. R. Kattner and C. E. Campbell, “Modelling of thermodynamics and diffusion in

multicomponent systems," *Mater. Sci. Technol.*, vol. 25, no. 4, pp. 443–459, 2009, doi: 10.1179/174328408X372001.

[28] P. Kejzlar, J. Machuta, and I. Nová, "Comparison of the structure of CuZn40MnAl alloy casted into sand and metal moulds," *Manuf. Technol.*, vol. 17, no. 1, pp. 44–48, 2017, doi: 10.21062/ujep/x.2017/a/1213-2489/mt/17/1/44.

[29] Y. Liu, L. Zhang, Y. Du, D. Yu, and D. Liang, "Atomic mobilities, uphill diffusion and proeutectic ferrite growth in Fe-Mn-C alloys," *Calphad Comput. Coupling Phase Diagrams Thermochem.*, vol. 33, no. 3, pp. 614–623, 2009, doi: 10.1016/j.calphad.2009.07.002.

[30] M. K. Toshinobu Nishibata, Takahiko Kohtake, "Kinetic Analysis of Uphill Diffusion of Carbon in Austenite Phase of Low-Carbon Steels," *Mater. Trans.*, vol. 61, no. 5, pp. 909–918, 2020.

[31] L. K. Zhang and B. R. Zhang, "Influence of multiphase microstructure evolution and Fe-rich phases on Cu uphill diffusion in Al-Si-Cu-Mg alloys," *Mater. Res. Express*, vol. 6, no. 11, 2019, doi: 10.1088/2053-1591/ab4490.

[32] V. B. Dung, "Uphill diffusion of Si-interstitial during boron diffusion in silicon," *Indian J. Phys.*, vol. 91, no. 10, pp. 1233–1236, 2017, doi: 10.1007/s12648-017-1024-0.

[33] L. S. Darken, "Diffusion of Carbon in Austenite with a Discontinuity of Composition," *Trans. AIME*, vol. Vol. 180, pp. 430–438, 1949.

[34] R. Krishna, "Uphill diffusion in multicomponent mixtures," *Chem. Soc. Rev.*, vol. 44, no. 10, pp. 2812–2836, 2015, doi: 10.1039/c4cs00440j.

[35] H. K. Badeshia, "Kirkendall Effect." https://www.phase-trans.msm.cam.ac.uk/kirkendall.html.

[36] K. Weinberg and T. Böhme, "Condensation and growth of Kirkendall voids in intermetallic compounds," *IEEE Trans. Components Packag. Technol.*, vol. 32, no. 3, pp. 684–692, 2009, doi: 10.1109/TCAPT.2008.2010057.

[37] H. H. Yao, A. D. Trigg, and C. T. Chong, "Substrate Interconnect," pp. 13–16.

[38] L. Sun, M. he Chen, L. Zhang, P. He, and L. sheng Xie, "Recent progress in SLID bonding in novel 3D-IC technologies," *J. Alloys Compd.*, vol. 818, no. October, p. 152825, 2020, doi: 10.1016/j.jallcom.2019.152825.

[39] B. H. L. Chao, X. Zhang, S. H. Chae, and P. S. Ho, "Recent advances on kinetic analysis of electromigration enhanced intermetallic growth and damage formation in Pb-free solder joints," *Microelectron. Reliab.*, vol. 49, no. 3, pp. 253–263, 2009, doi: 10.1016/j.microrel.2009.01.006.

[40] M. Han, "Copper wire bond pad/IMC interfacial layer crack study during HTSL (high temperature storage life) test," *IEEE 18th Electron. Packag. Technol. Conf.*, 2016.

[41] F. A. Shah, K. Ruscsák, and A. Palmquist, "50 Years of Scanning Electron Microscopy of Bone—a Comprehensive Overview of the Important Discoveries Made and Insights Gained Into Bone Material Properties in Health, Disease, and Taphonomy," *Bone Res.*, vol. 7, no. 1, pp. 1–15, 2019, doi: 10.1038/s41413-019-0053-z.

[42] M. C. Chen, C. W. Kuo, C. M. Chang, C. C. Hsieh, Y. Y. Chang, and W. Wu, “Diffusion and formation of intermetallic compounds during accumulative roll-bonding of Al/Mg alloys,” *Mater. Trans.*, vol. 48, no. 10, pp. 2595–2598, 2007, doi: 10.2320/matertrans.MD200718.

[43] G. Abbas Gohar, T. Manzoor, and A. N. Shah, “Investigation of thermal and mechanical properties of Cu-Al alloys with silver addition prepared by powder metallurgy,” *J. Alloys Compd.*, vol. 735, no. March 2019, pp. 802–812, 2018, doi: 10.1016/j.jallcom.2017.11.176.

[44] Amir Hossein Assari and Beitallah Eghbali, “Microstructure and Kinetics of Intermetallic Phase Formation during Solid State Diffusion Bonding in Bimetal Ti/Al,” *Phys. Met. Metallogr.*, vol. 120, no. 3, pp. 260–268, 2019, doi: 10.1134/S0031918X19030025.

BIOGRAPHICAL INFORMATION

Ratan Kota received his Bachelor of Technology degree in Metallurgical Engineering from Jawaharlal Nehru Technological University, India in 2016. He joined University of Texas at Arlington in 2018 to pursue his Master of Science degree in Materials Science and Engineering. He joined Prof. Choong-Un Kim's research group during his study at UT Arlington and worked on advanced structural materials. His research work is mainly focused on material characterization, diffusion, phase diagrams and heat treatment.